The University of Sydney

Department of Civil Engineering
Sydney NSW 2006
AUSTRALIA

http://www.civil.usyd.edu.au/

Centre for Advanced Structural Engineering

Isoparametric Spline Finite Strip Method for In-plane Stress Analysis

Research Report No. R848

Gabriele Eccher MEng
Kim J. R. Rasmussen MScEng PhD
Nadia Baldassino MEng
Riccardo Zandonini MEng PhD

August 2005

The University of Sydney

Department of Civil Engineering
Centre for Advanced Structural Engineering
http://www.civil.usyd.edu.au/

Isoparametric Spline Finite Strip Method for In-plane Stress Analysis

Research Report No. R848

Gabriele Eccher MEng
Kim J. R. Rasmussen MScEng PhD
Nadia Baldassino MEng
Riccardo Zandonini MEng PhD

August 2005

Abstract:

The finite strip method has proved to be an accurate and efficient tool for the analysis of structures having regular cross-section and mechanical proprieties along the longitudinal axis. The spline finite strip method has furthermore proved to be a more flexible tool for the analysis of structures with general support conditions and, utilising the isoparametric mapping, structures with a geometry varying along the longitudinal direction, such as curved slab bridges. In this report, the isoparametric spline finite strip method is applied to the analysis of plate containing cut-outs of different shape and subjected to in-plane stresses.
The mapping technique and the theory for the general in-plane stress condition are outlined, as is a novel method for assembling the strips in order to model the particular case of a cut-out.
To prove the reliability of the isoparametric spline finite strip method, three different shapes perforation in rectangular plates in traction are analysed. The shapes of the cut-outs presented are a circular, a rectangular and a key-shaped hole. The result are compared with exact solutions and finite element analyses.

Keywords:
isoparametric spline finite strip method, perforations, numerical analysis, thin-walled elements, plates, in-plane stress.

Copyright Notice

Department of Civil Engineering, Research Report R848
Isoparametric Spline Finite Strip Method for In-plane Stress Analysis

G.Eccher@civil.usyd.edu.au, K.Rasmussen@civil.usyd.edu.au, Nadia.Baldassino@ing.unitn.it and Riccardo.Zandonini@ing.unitn.it

Published by:
Department of Civil Engineering
The University of Sydney
Sydney NSW 2006
AUSTRALIA

August 2005

This report and other Research Reports published by The Department of Civil Engineering are available on the Internet:

http://www.civil.usyd.edu.au

TABLE OF CONTENTS

Isoparametric Spline Finite Strip Method for In-plane Stress Analysis

1- Introduction

The Spline Finite Strip Method was developed from the semi-analytical Finite Strip Method originally derived by Cheung (1976). The Finite Strip Method was based on harmonic functions, and proved to be an efficient tool for analysing structures with constant geometrical properties along a particular direction, generally the longitudinal one. The spline finite strip method complemented the finite strip method by allowing more complex types of loading and geometry to be modelled at the expense of a more comprehensive set of displacement functions based on splines. Initially introduced for the static analysis and free vibration of thin plates (Cheung, Fan et al. 1982), the spline finite strip method has been fully developed for the elastic structural analysis of folded plate structures (Fan 1982). The spline finite strip method was then extended to the buckling analysis of thin plates and folded-plate structures by Lau and Hancock (1986). The isoparametric concept was applied to the method for the analysis of Mindlin plate bending and plane stress plates (Au and Cheung 1993) and to degenerated shells (Cheung and Au 1995), providing narrow-banded matrices and, consequently, proving to be computationally efficient. The method has been applied, in the present work, to the analysis of thin plates with cut-outs. The research interest originates from the industrial and civil use of thin-walled structural members with perforations, which can be addressed as a complex system of thin plates. Holes and cut-outs of various shapes ease the assembly of the global structure without bolts or welds (Godley 1991), but introduce discontinuities in the cross-section and, consequently, a redistribution of the membrane stresses within the element (Baldassino, Eccher et al. 2005). Extensive research has been undertaken in the last decade studying the behaviour of thin plates containing cut-outs of different shape (Shanmugam, Thevendran et al. 1999), beams with holes in the web (Shanmugam and Thevendran 1991) and thin-walled members with cut-outs (Shanmugam and Dhanalakshmi 2001) highlighting the complexity of the analysis of such structures. The shape of the hole, its position within the cross-section, its dimensions and its longitudinal spacing (Rhodes and Macdonald 1996) are some of the most important parameters defining the global behaviour of the member but it is difficult to combine these factors to predict the loading capacity of such members with perforations. The design of perforated members is therefore traditionally carried out either by experimental or computer analysis, traditionally demanding finite elements.

Within this general framework, the primary objective of the present work is to present an efficient Spline Finite Strip Method (SFSM) for the accurate analysis of prismatic thin-walled structures characterised by a non-regular geometry and subjected to in-plane stress. For this purpose, an isoparametric mapping of the

geometry is developed and utilised. The reliability of the method is verified by analysing plates in tension containing circular, rectangular and key-shaped cut-outs.

2- Theory

The spline finite strip method described in the next chapters follows the finite strip theory (Cheung 1976). Similarly to the well-known finite element method (Zienkiewicz 1977), this approach subdivides the structural element in sub-domains and pre-defines displacement functions representing the deformed shape of the structure. The main difference between the finite strip and finite element methods lies in the shape of the elements and the choice of displacement functions. In the finite strip method, each sub-element is characterised by having a longitudinal dimension much larger that the other two, and, in general, extending the full length of the member. Within each element (or strip), the displacement functions are defined as a combination of a transverse shape set of polynomials (as in the finite element method) and by a longitudinal set of functions, which may vary from trigonometric series to eigen-functions and to spline series. The latter is the one considered in this work, utilising in particular the so-called B_3 cubic spline.

2.1- Shape Functions

An isoparametric cubic finite strip formulation is presented, implying that cubic polynomials are utilised both for the geometry description and for the displacement functions. Each strip is defined by four nodal lines which are subdivided in an arbitrary number (m) of sections. Fig. 1 shows a cubic strip with four longitudinal sections.
With regard to the longitudinal direction the B_3 cubic spline of unit length is employed, i.e.

$$\phi_i(\eta)=\frac{1}{6}\cdot\begin{cases}0 & , \quad \eta<\eta_{i-2}\\ (\eta-\eta_{i-2})^3 & , \quad \eta_{i-2}\le\eta<\eta_{i-1}\\ 1+3(\eta-\eta_{i-1})+3(\eta-\eta_{i-1})^2-3(\eta-\eta_{i-1})^3 & , \quad \eta_{i-1}\le\eta<\eta_i\\ 1+3(\eta_{i+1}-\eta)+3(\eta_{i+1}-\eta)^2-3(\eta_{i+1}-\eta)^3 & , \quad \eta_i\le\eta<\eta_{i+1}\\ (\eta_{i+2}-\eta)^3 & , \quad \eta_{i+1}\le\eta<\eta_{i+2}\\ 0 & , \quad \eta_{i+2}<\eta\end{cases} \qquad \text{Eq. 1}$$

In Eq. 1 $\phi_i(\eta)$ represents the i-th component of the cubic spline series, having non-zero values only over four consecutive sections centred over the i-th node, while η is the natural longitudinal coordinate. Fig. 2(a) shows the shape of the spline component while in Fig. 2(b) the full series is represented. The complete spline expansion comprises m+3 components, where m is the number of longitudinal subdivisions of the strip. It is worth noting that this gives rise to

m+1 nodes along each nodal line. In addition, two fictitious "extra nodes" per nodal line outside its boundaries are added to complete the series representation.

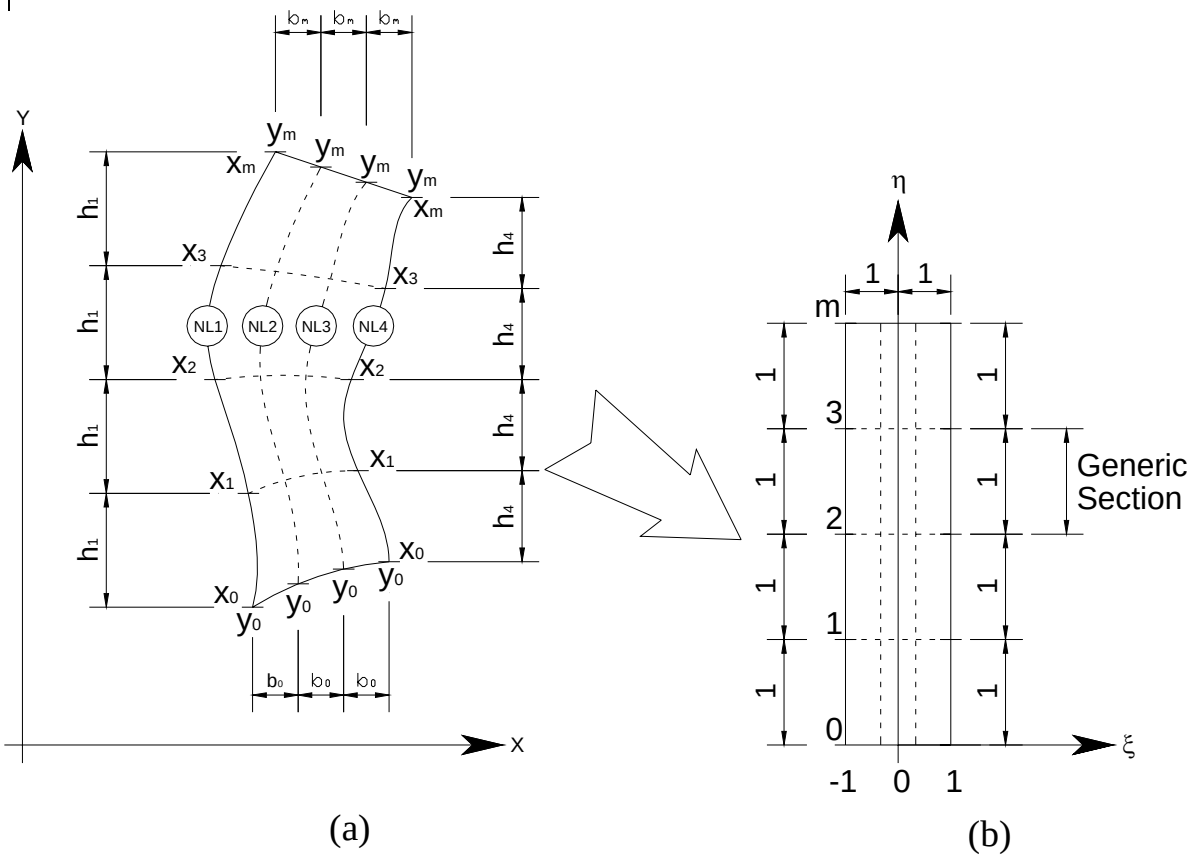

Fig. 1: (a) Generic cubic strip in the global coordinate system; (b) Generic strip mapped into the natural coordinate system.

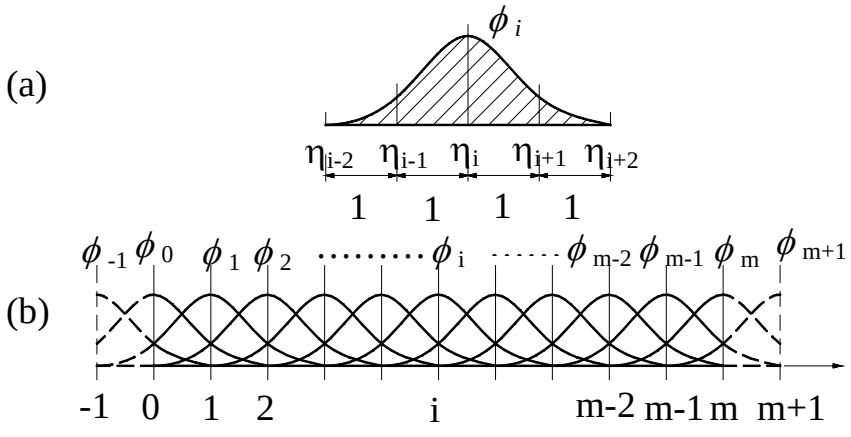

Fig. 2: (a) - ith component of the B3-Spline; (b) - a complete B_3-Spline.

In the transverse direction, represented by the natural coordinate ξ, cubic polynomial shape functions are utilised, i.e.

$$L_1(\xi) = -\frac{9}{16}\left(\xi^3 - \xi^2 - \frac{1}{9}\xi + \frac{1}{9}\right) \quad \text{Eq. 2}$$

$$L_2(\xi) = \frac{27}{16}\left(\xi^3 - \frac{1}{3}\xi^2 - \xi + \frac{1}{3}\right) \quad \text{Eq. 3}$$

$$L_3(\xi) = -\frac{27}{16}\left(\xi^3 + \frac{1}{3}\xi^2 - \xi - \frac{1}{3}\right) \quad \text{Eq. 4}$$

$$L_4(\xi) = \frac{9}{16}\left(\xi^3 + \xi^2 - \frac{1}{9}\xi - \frac{1}{9}\right) \quad \text{Eq. 5}$$

where $L_i(\xi)$ is the component of the shape functions referring to the i-th nodal line of the strip. A graphic representation of the transverse shape functions is given in Fig. 3.

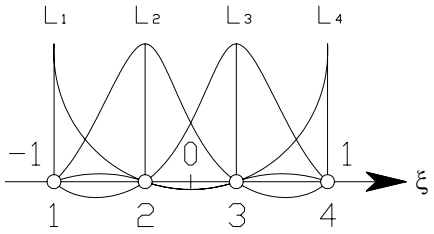

Fig. 3: Cubic transverse shape functions.

2.2- Mapping

The coordinates of the generic point P(x, y) within a strip are expressed in terms of the natural coordinates ξ and η as

$$x(\xi,\eta) = \sum_{i=1}^{4}\sum_{j=-1}^{m+1} L_i(\xi)\cdot\phi_j(\eta)\cdot\overline{\alpha}_{ij}^{x} \quad \text{Eq. 6}$$

$$y(\xi,\eta) = \sum_{i=1}^{4}\sum_{j=-1}^{m+1} L_i(\xi)\cdot\phi_j(\eta)\cdot\overline{\alpha}_{ij}^{y} \quad \text{Eq. 7}$$

where $\overline{\alpha}_{ij}^{x}$ and $\overline{\alpha}_{ij}^{y}$ are numerical coefficients to be determined from the geometry. They consist in 4(m+3) coefficients for each coordinate. For each node of the strip, $x_{ij}(\xi_i,\eta_j)$, $y_{ij}(\xi_i,\eta_j)$, it is possible to write the following relationships

$$x_{ij}(\xi_i,\eta_j) = L_i(\xi_i)\cdot\sum_{k=j-1}^{j+1}\phi_k(\eta_j)\cdot\bar{\alpha}^x_{ik} = \begin{bmatrix}\frac{1}{6} & \frac{2}{3} & \frac{1}{6}\end{bmatrix}\cdot\begin{bmatrix}\bar{\alpha}^x_{ij-1}\\ \bar{\alpha}^x_{ij}\\ \bar{\alpha}^x_{ij+1}\end{bmatrix} \qquad \textbf{Eq. 8}$$

$$y_{ij}(\xi_i,\eta_j) = L_i(\xi_i)\cdot\sum_{k=j-1}^{j+1}\phi_k(\eta_j)\cdot\bar{\alpha}^y_{ik} = \begin{bmatrix}\frac{1}{6} & \frac{2}{3} & \frac{1}{6}\end{bmatrix}\cdot\begin{bmatrix}\bar{\alpha}^y_{ij-1}\\ \bar{\alpha}^y_{ij}\\ \bar{\alpha}^y_{ij+1}\end{bmatrix} \qquad \textbf{Eq. 9}$$

It is possible to write 4(m+1) equations like these for each nodal line, while the remaining 8 conditions needed to define all the geometrical coefficients can be obtained either by specifying the global coordinates of the two extra points within each nodal line (corresponding to arbitrary values of η), or by prescribing the values of the derivatives of the coordinates at the extremes of each nodal line, i.e.

$$\frac{\partial x_{ij}}{\partial\eta}(\xi_i,\eta_j) = L_i(\xi_i)\cdot\sum_{k=j-1}^{j+1}\phi'_k(\eta_j)\cdot\bar{\alpha}^x_{ik} = \begin{bmatrix}-\frac{1}{2} & 0 & \frac{1}{2}\end{bmatrix}\cdot\begin{bmatrix}\bar{\alpha}^x_{ij-1}\\ \bar{\alpha}^x_{ij}\\ \bar{\alpha}^x_{ij+1}\end{bmatrix} \qquad \textbf{Eq. 10}$$

$$\frac{\partial y_{ij}}{\partial\eta}(\xi_i,\eta_j) = L_i(\xi_i)\cdot\sum_{k=j-1}^{j+1}\phi'_k(\eta_j)\cdot\bar{\alpha}^y_{ik} = \begin{bmatrix}-\frac{1}{2} & 0 & \frac{1}{2}\end{bmatrix}\cdot\begin{bmatrix}\bar{\alpha}^y_{ij-1}\\ \bar{\alpha}^y_{ij}\\ \bar{\alpha}^y_{ij+1}\end{bmatrix} \qquad \textbf{Eq. 11}$$

In order to ease the geometry definition, it may be noted that not all the 4(m+3) coefficients for each coordinate have to be explicitly specified. Concentrating on a particular nodal line, it may be observed that if the inner nodes are sampled as shown in Fig. 1(a), i.e. at a constant y-spacing h_i, only the x-coordinate values of the nodes have to be prescribed, while for the y-coordinate it is possible to establish a linear variation between the y-values assumed at the extremes of each nodal line, y_{im} and y_{i0}, i.e.

$$y_i(\xi_i,\eta) = y_{i0} + \frac{y_{im}-y_{i0}}{m}\cdot\eta; \qquad (i = 1,\ldots,4) \qquad \textbf{Eq. 12}$$

Similarly, for the transverse edges of the strip (corresponding to $\eta = 0$ and $\eta = m$), if the nodes are sampled at a constant spacing (b_0 or b_m in Fig. 1(a)), then only the y-coordinates of the intermediate nodes (i.e. for the second and the third nodal line) have to be specified, while for the x-coordinate the following holds

$$x(\xi,\eta_k) = x_{1k} + \frac{x_{4k}-x_{1k}}{2}\cdot(\xi+1); \qquad (k = 0,m) \qquad \textbf{Eq. 13}$$

The same interpolation can be made for the x-coordinates of the inner nodes in terms of the x-coordinates of the longitudinal nodal lines x_{1j} and x_{4j}, j = 1,2,…,m-1. With those assumption it is possible to fully describe the geometry of the strip by simply prescribing:

- x nodal coordinates along the longitudinal boundary;
- y nodal coordinates along the transverse edges of the strip.

Solving the linear system obtained from the appropriate combination of equations Eq. 8 to Eq. 11 for the values of the geometrical coefficients $\bar{\alpha}_{ij}^{x}$ and $\bar{\alpha}_{ij}^{y}$, the mapping functions may be expressed as

$$x(\xi,\eta) = \sum_{j=-1}^{m+1} \phi_j(\eta)\left(\bar{\alpha}_{1j}^{x} + \frac{\bar{\alpha}_{4j}^{x} - \bar{\alpha}_{1j}^{x}}{2}(\xi+1)\right) \qquad \textbf{Eq. 14}$$

$$y(\xi,\eta) = \sum_{i=1}^{4} L_i(\xi)\left(y_{i0} + \frac{y_{im} - y_{i0}}{m}\eta\right) \qquad \textbf{Eq. 15}$$

In practical applications, due to the cubic nature of the mapping functions, a few sections, e.g. one or two, may be sufficient to describe intricate geometries, while the complexity of the stress distribution may require a much higher number of sections for the displacement field. It may be noted that for fine meshes, i.e. high values for the parameter m, the definition of geometrical coordinates becomes tedious. It is therefore useful to define the geometrical discretisation independently of the mesh utilised for the structural analysis, i.e. having different values for the m used in the geometry description, m_g, and the m used for the displacement functions, m_s. This can be easily achieved without loosing the isoparametric nature of the method if the number of geometrical nodes is artificially augmented from m_g+3 to m_s+3 nodes per nodal line. While for Eq. 15 is straightforward to change from an m_g discretisation to an m_s discretisation simply by changing the value of m; in Eq. 14 it is firstly necessary to transform the m_g+3 set of coefficients to a new set of m_s+3 per nodal line. The function describing the x-coordinate along the i-th nodal line defined over m_s sections can be expressed as

$$x_{ij}(\xi_i,\eta_j) = \sum_{k=j-1}^{j+1} \phi_k(j)\cdot\bar{\beta}_{ik}^{x} = \begin{bmatrix} \frac{1}{6} & \frac{2}{3} & \frac{1}{6} \end{bmatrix}\cdot\begin{bmatrix} \bar{\beta}_{ij-1}^{x} \\ \bar{\beta}_{ij}^{x} \\ \bar{\beta}_{ij+1}^{x} \end{bmatrix}; \quad (j = 0,1,\ldots,m_s) \qquad \textbf{Eq. 16}$$

while the same function expressed in terms of m_g sections and $\bar{\alpha}_{ij}^{x}$ coefficients is

$$x_{ij}(\xi_i,\eta_j)=\sum_{k=j^- -1}^{j^+ +1}\phi_k(\tilde{j})\cdot\overline{\alpha}^x_{ik}=\left[\phi_{j^- -1}(\tilde{j})\quad\phi_{j^-}(\tilde{j})\quad\phi_{j^+}(\tilde{j})\quad\phi_{j^+ +1}(\tilde{j})\right]\cdot\begin{bmatrix}\overline{\alpha}^x_{ij^- -1}\\ \overline{\alpha}^x_{ij^-}\\ \overline{\alpha}^x_{ij^+}\\ \overline{\alpha}^x_{ij^+ +1}\end{bmatrix};\quad (j=0,1,\ldots,m_s) \qquad \textbf{Eq. 17}$$

where

$$\tilde{j}=\frac{m_g}{m_s}\cdot j;\quad j^-=floor(j);\quad j^+=ceiling(j)$$

Repeating the same procedure with regard to the derivative over the natural coordinate η, for both representation we get

$$\frac{\partial x_{ij}(\xi_i,\eta_j)}{\partial\eta}=\sum_{k=j-1}^{j+1}\phi'_k(j)\cdot\overline{\beta}^x_{ik}=\left[-\frac{1}{2}\quad 0\quad\frac{1}{2}\right]\cdot\begin{bmatrix}\overline{\beta}^x_{ij-1}\\ \overline{\beta}^x_{ij}\\ \overline{\beta}^x_{ij+1}\end{bmatrix};\quad (j=0,1,\ldots,m_s) \qquad \textbf{Eq. 18}$$

and

$$\frac{\partial x_{ij}(\xi_i,\eta_j)}{\partial\eta}=\sum_{k=j^- -1}^{j^+ +1}\frac{m_s}{m_g}\cdot\phi'_k(\tilde{j})\cdot\overline{\alpha}^x_{ik}=\frac{m_s}{m_g}\cdot\left[\phi'_{j^- -1}(\tilde{j})\quad\phi'_{j^-}(\tilde{j})\quad\phi'_{j^+}(\tilde{j})\quad\phi'_{j^+ +1}(\tilde{j})\right]\cdot\begin{bmatrix}\overline{\alpha}^x_{ij^- -1}\\ \overline{\alpha}^x_{ij^-}\\ \overline{\alpha}^x_{ij^+}\\ \overline{\alpha}^x_{ij^+ +1}\end{bmatrix};\quad (j=0,1,\ldots,m_s) \qquad \textbf{Eq. 19}$$

By equating Eq. 16 with Eq. 17 for j = 0,1,…,m_s and Eq. 18 with Eq. 9 for j = 0, m_s, it is possible to derive a system of m_s+3 linearly independent equations in the m_s+3 $\overline{\beta}^x_{ik}$ coefficients, i.e.

$$\left[\frac{1}{6}\quad\frac{2}{3}\quad\frac{1}{6}\right]\cdot\begin{bmatrix}\overline{\beta}^x_{ij-1}\\ \overline{\beta}^x_{ij}\\ \overline{\beta}^x_{ij+1}\end{bmatrix}=\left[\phi_{j^- -1}(\tilde{j})\quad\phi_{j^-}(\tilde{j})\quad\phi_{j^+}(\tilde{j})\quad\phi_{j^+ +1}(\tilde{j})\right]\cdot\begin{bmatrix}\overline{\alpha}^x_{ij^- -1}\\ \overline{\alpha}^x_{ij^-}\\ \overline{\alpha}^x_{ij^+}\\ \overline{\alpha}^x_{ij^+ +1}\end{bmatrix};\quad (j=0,1,\ldots,m_s) \qquad \textbf{Eq. 20}$$

$$\left[-\frac{1}{2}\quad 0\quad\frac{1}{2}\right]\cdot\begin{bmatrix}\overline{\beta}^x_{ij-1}\\ \overline{\beta}^x_{ij}\\ \overline{\beta}^x_{ij+1}\end{bmatrix}=\frac{m_s}{m_g}\cdot\left[\phi'_{j^- -1}(\tilde{j})\quad\phi'_{j^-}(\tilde{j})\quad\phi'_{j^+}(\tilde{j})\quad\phi'_{j^+ +1}(\tilde{j})\right]\cdot\begin{bmatrix}\overline{\alpha}^x_{ij^- -1}\\ \overline{\alpha}^x_{ij^-}\\ \overline{\alpha}^x_{ij^+}\\ \overline{\alpha}^x_{ij^+ +1}\end{bmatrix};\quad (j=0,m_s) \qquad \textbf{Eq. 21}$$

Eq. 14 and Eq. 15 can now be expressed in terms of m_s sections as

$$x(\xi,\eta)=\sum_{j=-1}^{m_s+1}\phi_j(\eta)\left(\overline{\beta}_{1j}^{x}+\frac{\overline{\beta}_{4j}^{x}-\overline{\beta}_{1j}^{x}}{2}(\xi+1)\right) \quad \text{Eq. 22}$$

$$y(\xi,\eta)=\sum_{i=1}^{4}L_i(\xi)\left(y_{i0}+\frac{y_{im}-y_{i0}}{m_s}\eta\right) \quad \text{Eq. 23}$$

2.3- Plane Stress Analysis

The plane stress state can be fully represented by means of the two in-plane displacements, *u* and *v*, in the global x and the global y axis directions respectively. In terms of displacement functions (L_i, ϕ_j) and generalised displacements (α_{ij}) they can be expressed as

$$u(\xi,\eta)=\sum_{i=1}^{4}\sum_{j=-1}^{m_s+1}L_i(\xi)\cdot\phi_j(\eta)\cdot\alpha_{ij}^{u} \quad \text{Eq. 24}$$

$$v(\xi,\eta)=\sum_{i=1}^{4}\sum_{j=-1}^{m_s+1}L_i(\xi)\cdot\phi_j(\eta)\cdot\alpha_{ij}^{v} \quad \text{Eq. 25}$$

It is convenient to present the matrix formulation for the displacement field, **u**

$$\mathbf{u}=\mathbf{N}\cdot\boldsymbol{\alpha} \quad \text{Eq. 26}$$

where

$$\mathbf{u}=\mathbf{u}(\xi,\eta)=\begin{bmatrix}u(\xi,\eta)\\ v(\xi,\eta)\end{bmatrix} \quad \text{Eq. 27}$$

$$\mathbf{N}=\begin{bmatrix}\mathbf{N}_1 & 0 & \mathbf{N}_2 & 0 & \mathbf{N}_3 & 0 & \mathbf{N}_4 & 0\\ 0 & \mathbf{N}_1 & 0 & \mathbf{N}_2 & 0 & \mathbf{N}_3 & 0 & \mathbf{N}_4\end{bmatrix} \quad \text{Eq. 28}$$

where the generic sub-matrix $\mathbf{N}_i$ is given by

$$\mathbf{N}_i=L_i(\xi)\cdot\left[\phi_{-1}(\eta)\ \ \phi_0(\eta)\ \ \phi_1(\eta)\ \ \cdots\ \ \phi_{m_s}(\eta)\ \ \phi_{m_s+1}(\eta)\right] \quad \text{Eq. 29}$$

and $\boldsymbol{\alpha}$, expressed by

$$\boldsymbol{\alpha}=\left[\alpha_{1-1}^{u}\ \cdots\ \alpha_{1m+1}^{u}\ \ \alpha_{1-1}^{v}\ \cdots\ \alpha_{1m+1}^{v}\ \ \alpha_{2-1}^{u}\ \cdots\ \alpha_{2m+1}^{u}\ \ \alpha_{2-1}^{v}\ \cdots\ \alpha_{2m+1}^{v}\ \ \cdots\right.$$
$$\left.\cdots\ \ \alpha_{3-1}^{u}\ \cdots\ \alpha_{3m+1}^{u}\ \ \alpha_{3-1}^{v}\ \cdots\ \alpha_{3m+1}^{v}\ \ \alpha_{4-1}^{u}\ \cdots\ \alpha_{4m+1}^{u}\ \ \alpha_{4-1}^{v}\ \cdots\ \alpha_{4m+1}^{v}\right]^{T} \quad \text{Eq. 30}$$

represents the vector of unknown coefficients.

Following the chain rule, the linear strain-displacement relationship is obtained as

$$\boldsymbol{\varepsilon} = \begin{Bmatrix} \varepsilon_x \\ \varepsilon_y \\ \gamma_{xy} \end{Bmatrix} = \begin{Bmatrix} \dfrac{\partial u}{\partial x} \\ \dfrac{\partial v}{\partial y} \\ \dfrac{\partial u}{\partial y} + \dfrac{\partial v}{\partial x} \end{Bmatrix} = \begin{Bmatrix} \dfrac{\partial u}{\partial \xi}\dfrac{\partial \xi}{\partial x} + \dfrac{\partial u}{\partial \eta}\dfrac{\partial \eta}{\partial x} \\ \dfrac{\partial v}{\partial \xi}\dfrac{\partial \xi}{\partial y} + \dfrac{\partial v}{\partial \eta}\dfrac{\partial \eta}{\partial y} \\ \left(\dfrac{\partial u}{\partial \xi}\dfrac{\partial \xi}{\partial y} + \dfrac{\partial u}{\partial \eta}\dfrac{\partial \eta}{\partial y}\right) + \left(\dfrac{\partial v}{\partial \xi}\dfrac{\partial \xi}{\partial x} + \dfrac{\partial v}{\partial \eta}\dfrac{\partial \eta}{\partial x}\right) \end{Bmatrix} \quad \text{Eq. 31}$$

Introducing the general displacement δ we have

$$\frac{\partial \delta}{\partial \xi} = \sum_{i=1}^{4}\sum_{j=-1}^{m_s+1} L_i'(\xi)\cdot\phi_j(\eta)\cdot\alpha_{ij}^{\delta}; \quad (\delta = u, v) \quad \text{Eq. 32}$$

$$\frac{\partial \delta}{\partial \eta} = \sum_{i=1}^{4}\sum_{j=-1}^{m_s+1} L_i(\xi)\cdot\phi_j'(\eta)\cdot\alpha_{ij}^{\delta}; \quad (\delta = u, v) \quad \text{Eq. 33}$$

where

$$L_i'(\xi) = \frac{dL_i(\xi)}{d\xi} \quad \text{Eq. 34}$$

$$\phi_j'(\eta) = \frac{d\phi_j(\eta)}{d\eta} \quad \text{Eq. 35}$$

while the quantities $\frac{\partial \xi}{\partial x}, \frac{\partial \eta}{\partial x}, \frac{\partial \xi}{\partial y}$ and $\frac{\partial \eta}{\partial y}$ can be obtained from the Jacobian matrix of the mapping functions Eq. 22 and 23, i.e.

$$\begin{bmatrix} \dfrac{\partial \xi}{\partial x} & \dfrac{\partial \eta}{\partial x} \\ \dfrac{\partial \xi}{\partial y} & \dfrac{\partial \eta}{\partial y} \end{bmatrix} = \begin{bmatrix} \dfrac{\partial x}{\partial \xi} & \dfrac{\partial y}{\partial \xi} \\ \dfrac{\partial x}{\partial \eta} & \dfrac{\partial y}{\partial \eta} \end{bmatrix}^{-1} = \mathbf{J}^{-\mathsf{T}} \quad \text{Eq. 36}$$

The components of the inverse Jacobian matrix can be explicitly expressed as follows

$$\frac{\partial x(\xi,\eta)}{\partial \xi} = \sum_{j=-1}^{m_s+1}\left(\phi_j(\eta)\cdot\frac{\overline{\beta}_{4j}^{x} - \overline{\beta}_{1j}^{x}}{2}\right) \quad \text{Eq. 37}$$

$$\frac{\partial x(\xi,\eta)}{\partial \eta} = \sum_{j=-1}^{m_s+1}\phi_j'(\eta)\left(\overline{\beta}_{1j}^{x} + \frac{\overline{\beta}_{4j}^{x} - \overline{\beta}_{1j}^{x}}{2}(\xi+1)\right) \quad \text{Eq. 38}$$

$$\frac{\partial y(\xi,\eta)}{\partial \xi} = \sum_{i=1}^{4} L_i'(\xi)\left(y_{i0} + \frac{y_{im} - y_{i0}}{m_s}\eta \right) \quad \text{Eq. 39}$$

$$\frac{\partial y(\xi,\eta)}{\partial \eta} = \sum_{i=1}^{4}\left(L_i(\xi)\cdot \frac{y_{im} - y_{i0}}{m_s} \right) \quad \text{Eq. 40}$$

It is convenient to express Eq. 31 in terms of a strain matrix, **B**, and the vector **α** containing the generalised displacements,

$$\boldsymbol{\varepsilon} = \mathbf{B}\cdot\boldsymbol{\alpha} \quad \text{Eq. 41}$$

where

$$\mathbf{B} = \begin{bmatrix} \mathbf{B}_{1,x} & 0 & \mathbf{B}_{2,x} & 0 & \mathbf{B}_{3,x} & 0 & \mathbf{B}_{4,x} & 0 \\ 0 & \mathbf{B}_{1,y} & 0 & \mathbf{B}_{2,y} & 0 & \mathbf{B}_{3,y} & 0 & \mathbf{B}_{4,y} \\ \mathbf{B}_{1,y} & \mathbf{B}_{1,x} & \mathbf{B}_{2,y} & \mathbf{B}_{2,x} & \mathbf{B}_{3,y} & \mathbf{B}_{3,x} & \mathbf{B}_{4,y} & \mathbf{B}_{4,x} \end{bmatrix} \quad \text{Eq. 42}$$

where the j-th component of the row matrices $\mathbf{B}_{i,x}$ and $\mathbf{B}_{i,y}$ are given by

$$\left(\mathbf{B}_{i,x}\right)_j = L_i'(\xi)\cdot\phi_j(\eta)\cdot\frac{\partial\xi}{\partial x} + L_i\cdot(\xi)\cdot\phi_j'(\eta)\cdot\frac{\partial\eta}{\partial x} \quad \text{Eq. 43}$$

$$\left(\mathbf{B}_{i,y}\right)_j = L_i'(\xi)\cdot\phi_j(\eta)\cdot\frac{\partial\xi}{\partial y}\cdot + L_i(\xi)\cdot\phi_j'(\eta)\cdot\frac{\partial\eta}{\partial y} \quad \text{Eq. 44}$$

Applying the constitutive matrix, **D**, to the strain field, **ε**, the stress field, **σ**, is obtained as

$$\boldsymbol{\sigma} = \mathbf{D}\cdot\boldsymbol{\varepsilon} = \mathbf{D}\cdot\mathbf{B}\cdot\boldsymbol{\alpha} \quad \text{Eq. 45}$$

where

$$\boldsymbol{\sigma} = \begin{bmatrix} \sigma_x \\ \sigma_y \\ \tau_{xy} \end{bmatrix} \quad \text{Eq. 46}$$

and for an isotropic material in a state of plane stress with elastic modulus, *E*, and Poisson's ratio, *ν*, the constitutive matrix becomes

$$\mathbf{D} = \frac{E}{1-\nu^2}\begin{bmatrix} 1 & \nu & 0 \\ \nu & 1 & 0 \\ 0 & 0 & \frac{1}{2}(1-\nu) \end{bmatrix} \qquad \text{Eq. 47}$$

The elastic deformation energy of the strip, U_s, may be expressed as

$$\begin{aligned} U_s &= \frac{1}{2}\cdot\int_V \boldsymbol{\sigma}^T\cdot\boldsymbol{\varepsilon}\cdot dV = \frac{1}{2}\cdot t\cdot\int_A \boldsymbol{\sigma}^T\cdot\boldsymbol{\varepsilon}\cdot dA = \frac{1}{2}\cdot t\cdot\int_{-1}^{1}\int_0^{m_s}\boldsymbol{\sigma}^T\cdot\boldsymbol{\varepsilon}\cdot\det(\mathbf{J})\cdot d\eta\cdot d\xi \\ &= \frac{1}{2}\cdot\boldsymbol{\alpha}^T\cdot\left(t\int_{-1}^{1}\int_0^{m_s}\mathbf{B}^T\cdot\mathbf{D}\cdot\mathbf{B}\cdot\det(\mathbf{J})\cdot d\eta\cdot d\xi\right)\cdot\boldsymbol{\alpha} \\ &= \frac{1}{2}\cdot\boldsymbol{\alpha}^T\cdot\mathbf{K}_s\cdot\boldsymbol{\alpha} \end{aligned} \qquad \text{Eq. 48}$$

where the stiffness matrix $\mathbf{K}_s$ is defined as

$$\mathbf{K}_s = t\int_{-1}^{1}\int_0^{m_s}\mathbf{B}^T\cdot\mathbf{D}\cdot\mathbf{B}\cdot\det(\mathbf{J})\cdot d\eta\cdot d\xi \qquad \text{Eq. 49}$$

and t is assumed to be the uniform thickness of the strip.
Similarly the general expression for the potential energy of the external loads, V_s, is given by

$$\begin{aligned} V_s &= \int_V \mathbf{u}^T\cdot\mathbf{p}\cdot dV = t\cdot\int_A \mathbf{u}^T\cdot\mathbf{p}\cdot dA = t\cdot\int_{-1}^{1}\int_0^{m_s}\mathbf{u}^T\cdot\mathbf{p}\cdot\det(\mathbf{J})\cdot d\eta\cdot d\xi \\ &= \boldsymbol{\alpha}^T\cdot\left(t\int_{-1}^{1}\int_0^{m_s}\mathbf{N}^T\cdot\mathbf{p}\cdot\det(\mathbf{J})\cdot d\eta\cdot d\xi\right) \\ &= \boldsymbol{\alpha}^T\cdot\mathbf{v}_s \end{aligned} \qquad \text{Eq. 50}$$

where the vector **p** contains the external body force components parallel to the global axes, i.e.

$$\mathbf{p} = \mathbf{p}(\xi,\eta) = \begin{bmatrix} p_x(\xi,\eta) \\ p_y(\xi,\eta) \end{bmatrix} \qquad \text{Eq. 51}$$

while the equivalent force vector is defined as

$$\mathbf{v}_s = t\int_{-1}^{1}\int_0^{m_s}\mathbf{N}^T\cdot\mathbf{p}\cdot\det(\mathbf{J})\cdot d\eta\cdot d\xi \qquad \text{Eq. 52}$$

This general definition for **v** can be specialised to the different load types, i.e. body, surface, line and point loads. Introducing **b** for the equivalent force vector when **p** refers to body loads, the integration provides

$$\mathbf{b} = t\int_{-1}^{1}\int_{0}^{m_s} \mathbf{N}^T \cdot \mathbf{p} \cdot \det(\mathbf{J}) \cdot d\eta \cdot d\xi \qquad \textbf{Eq. 53}$$

If we consider surface tractions, the equivalent load vector (**s**) is,

$$\mathbf{s} = \int_{-1}^{1}\int_{0}^{m_s} \mathbf{N}^T \cdot \mathbf{p} \cdot \det(\mathbf{J}) \cdot d\eta \cdot d\xi \qquad \textbf{Eq. 54}$$

while for line loads along the natural coordinate ξ at given $\eta = \bar{\eta}$, we obtain the vector $\mathbf{l}_\xi$ as,

$$\mathbf{p} = \mathbf{p}\left(\xi, \bar{\eta}\right) = \begin{bmatrix} p_x\left(\xi, \bar{\eta}\right) \\ p_y\left(\xi, \bar{\eta}\right) \end{bmatrix} \qquad \textbf{Eq. 55}$$

$$\mathbf{l}_\xi = \int_{-1}^{1} \mathbf{N}^T \cdot \mathbf{p} \cdot ds_\xi \cdot d\xi \qquad \textbf{Eq. 56}$$

where

$$ds_\xi = ds_\xi\left(\xi, \bar{\eta}\right) = \sqrt{\left(\frac{\partial x\left(\xi, \bar{\eta}\right)}{\partial \xi}\right)^2 + \left(\frac{\partial y\left(\xi, \bar{\eta}\right)}{\partial \xi}\right)^2} \qquad \textbf{Eq. 57}$$

A line load developing along the natural coordinate η at given $\xi = \bar{\xi}$ can be expressed as ($\mathbf{l}_\eta$),

$$\mathbf{p} = \mathbf{p}\left(\bar{\xi}, \eta\right) = \begin{bmatrix} p_x\left(\bar{\xi}, \eta\right) \\ p_y\left(\bar{\xi}, \eta\right) \end{bmatrix} \qquad \textbf{Eq. 58}$$

$$\mathbf{l}_\eta = \int_{0}^{m_s} \mathbf{N}^T \cdot \mathbf{p} \cdot ds_\eta \cdot d\eta \qquad \textbf{Eq. 59}$$

where

$$ds_\eta = ds_\eta\left(\bar{\xi}, \eta\right) = \sqrt{\left(\frac{\partial x\left(\bar{\xi}, \eta\right)}{\partial \eta}\right)^2 + \left(\frac{\partial y\left(\bar{\xi}, \eta\right)}{\partial \eta}\right)^2} \qquad \textbf{Eq. 60}$$

In the case of a point load, where the integration reduces to the evaluation of the integrating functions at the point of loading $(\bar{\xi},\bar{\eta})$, the equivalent force vector (**c**) becomes,

$$\mathbf{p} = \mathbf{p}(\bar{\xi},\bar{\eta}) = \begin{bmatrix} p_x(\bar{\xi},\bar{\eta}) \\ p_y(\bar{\xi},\bar{\eta}) \end{bmatrix} \quad \text{Eq. 61}$$

$$\mathbf{c} = \mathbf{N}^T(\bar{\xi},\bar{\eta}) \cdot \mathbf{p}(\bar{\xi},\bar{\eta}) \quad \text{Eq. 62}$$

We may express then the final equivalent force vector as the summation of the contributions of the different load types, i.e.

$$\mathbf{v}_S = \mathbf{b} + \mathbf{s} + \mathbf{l}_\xi + \mathbf{l}_\eta + \mathbf{c} \quad \text{Eq. 63}$$

The total potential energy of the strip is expressed by

$$\Pi_S = U_S + V_S \quad \text{Eq. 64}$$

and can be rewritten in matrix form as

$$\Pi_S = \frac{1}{2} \cdot \boldsymbol{\alpha}^T \cdot \mathbf{K}_S \cdot \boldsymbol{\alpha} - \boldsymbol{\alpha}^T \cdot \mathbf{v}_S \quad \text{Eq. 65}$$

The potential energy for the entire structure can be obtained by the well-known assembling process, which consists of adding the stiffness matrix, $\mathbf{K}_S$, and the load vector contributions, $\mathbf{v}_S$, of each strip into the global matrices, **K** and **v** to obtain the total potential energy of the structure, e.g.

$$\Pi = \frac{1}{2} \cdot \boldsymbol{\alpha}^T \cdot \mathbf{K} \cdot \boldsymbol{\alpha} - \boldsymbol{\alpha}^T \cdot \mathbf{v} \quad \text{Eq. 66}$$

where

$$\mathbf{K} = \text{"}\sum \mathbf{K}_s\text{"} \quad \text{Eq. 67}$$

$$\mathbf{v} = \text{"}\sum \mathbf{v}_s\text{"} \quad \text{Eq. 68}$$

where the summations in Eq 67 and Eq 68 stand for the assembling process and $\boldsymbol{\alpha}$ represents now the unknown vector of the entire structure.
The equilibrium condition $\delta\prod = 0$ provides the usual linear system in the unknown vector $\boldsymbol{\alpha}$, i.e.

$$\mathbf{K} \cdot \boldsymbol{\alpha} = \mathbf{v} \qquad \text{Eq. 69}$$

3- Modelling Considerations

In order to represent a discontinuity like a hole, in addition to the standard finite strip assembling process, it is also necessary to assemble longitudinally different sets of strips.

Fig. 4 represents a plate containing a hole. A possible longitudinal strip configuration is shown in Fig. 4(a), and it is clear that the coordinates of the longitudinal edge of a strip encounter a discontinuity in their first derivatives when the edge reaches a hole (e.g. nodal line 3 or nodal line 4 in Fig. 4(a)). The C_2 continuity characterising the B_3 spline cannot accommodate such discontinuities and is therefore necessary to split the longitudinal discretisation in more that one set of parallel strip (Fig. 4(b)).

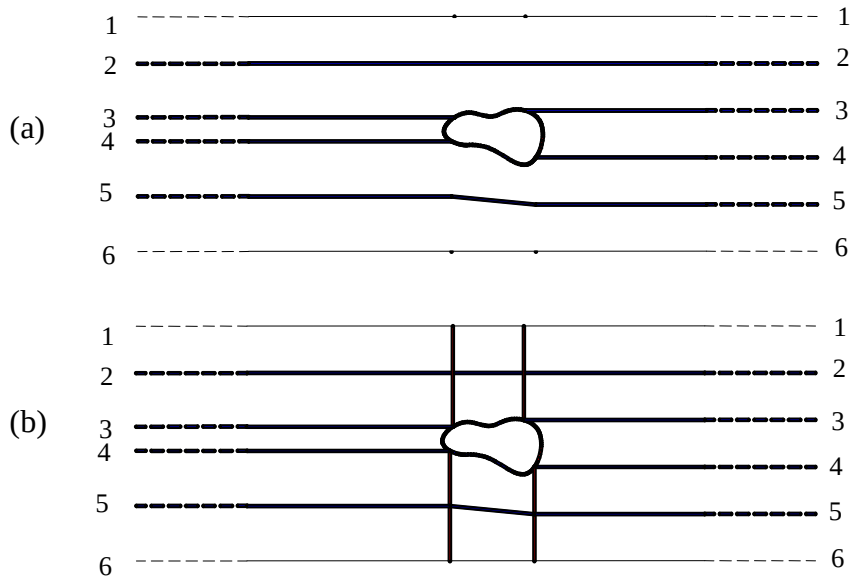

Fig. 4: (a) Transverse strip discretisation of a region with a hole; (b) Transverse and longitudinal strip discretisation of a region with a hole.

This implies that the stiffness contributions from adjacent strips in the longitudinal direction have to be assembled to ensure continuity in the displacement variables and their derivatives. For this purpose, some of the spline coefficients contained in the unknown vector $\boldsymbol{\alpha}$ have to be transformed into physical parameters like displacements, δ, or their derivatives, $\frac{\partial \delta}{\partial x}$, $\frac{\partial \delta}{\partial y}$, $\frac{\partial \delta}{\partial \xi}$ or $\frac{\partial \delta}{\partial \eta}$, evaluated along the adjoining transverse edges. In particular, for the present work, the continuity in the displacements *u* and *v* as well as in their first derivatives with respect to the longitudinal global y-coordinate, $\frac{\partial u}{\partial y}$ and $\frac{\partial v}{\partial y}$,

have been required, unless otherwise specified by support conditions along the transverse edge.
In the following sections, a general method for transforming the spline coefficients into physical ones is introduced. A further explanation why the longitudinal assembly is only required to ensure continuity between displacements and their first derivatives in y is also provided.

3.1- Longitudinal Assembly of Strips and Boundary conditions

As previously mentioned, to provide continuity between displacement and rotations across two adjoining strips, a transformation of some of the nodal parameters is required.
If no support conditions are prescribed along the transverse edge, the first ($\alpha^i_{-1}, \alpha^i_0$) and last ($\alpha^i_m, \alpha^i_{m+1}$) two node parameters of the spline functions are transformed into displacements and into the derivatives of the displacements in the y-direction, as follows:

$$\begin{aligned} \alpha^i_{-1} &\rightarrow \frac{\partial \delta^i_0}{\partial y} \\ \alpha^i_0 &\rightarrow \delta^i_0 \\ \alpha^i_m &\rightarrow \frac{\partial \delta^i_m}{\partial y} \\ \alpha^i_{m+1} &\rightarrow \delta^i_m \end{aligned} \qquad \text{Eq. 70}$$

where with δ we may represent the generic degree of freedom, i.e. *u* or *v*.
If support conditions are prescribed along the transverse edge, the first (α^i_{-1}) and the second last (α^i_m) conditions shown in Eq. 70 are changed into:

$$\begin{aligned} \alpha^i_{-1} &\rightarrow \frac{\partial \delta^i_0}{\partial x} \quad \text{or} \quad \frac{\partial \delta^i_0}{\partial \eta} \\ \alpha^i_m &\rightarrow \frac{\partial \delta^i_m}{\partial x} \quad \text{or} \quad \frac{\partial \delta^i_m}{\partial \eta} \end{aligned} \qquad \text{Eq. 71}$$

It should be pointed out that any condition in the derivative of the displacement with regard to the transverse natural coordinate, ξ, along the transverse edges of a strip, e.g. $\frac{\partial \delta}{\partial \xi}$, can be easily expressed in terms of the displacements (δ_i) of the nodal lines: by evaluating Eq. 24 (or Eq. 25) on the i-th nodal line, i.e.

$$\begin{aligned} \delta_i = \delta(\xi_i) &= \sum_{i=1}^{4} \sum_{j=-1}^{m_s+1} L_i(\xi_i) \cdot \phi_j(\eta) \cdot \alpha^{\delta}_{ij} \; ; \quad (\delta = u, v) \\ &= \sum_{j=-1}^{m_s+1} \phi_j(\eta) \cdot \alpha^{\delta}_{ij} \end{aligned} \qquad \text{Eq. 72}$$

and comparing Eq. 72 with Eq. 32 it is clear that $\frac{\partial \delta}{\partial \xi}$ evaluated at the extreme end of each line can be represented as a linear combination of that specific displacement (δ_i, i=1,2,..,4) evaluated at the corresponding end of each nodal line of the strip.
Independently of the assembling process, it is possible to apply any boundary conditions over the generic internal node, *j*, of the generic line, *i*, as:

$$\alpha_j^i \rightarrow \delta_j^i \quad \text{or} \quad \frac{\partial \delta_j^i}{\partial \xi} \quad \text{or} \quad \frac{\partial \delta_j^i}{\partial \eta} \quad \text{or} \quad \frac{\partial \delta_j^i}{\partial x} \quad \text{or} \quad \frac{\partial \delta_0^i}{\partial y} \qquad \textbf{Eq. 73}$$

For the sake of convenience, we may give arbitrary names to the boundary condition types, i.e.,

Name	Bc1	Bc2	Bc3	Bc4	Bc5
Parameter	δ_j^i	$\frac{\partial \delta_j^i}{\partial \xi}$	$\frac{\partial \delta_j^i}{\partial \eta}$	$\frac{\partial \delta_j^i}{\partial x}$	$\frac{\partial \delta_j^i}{\partial y}$

Table 1: Boundary conditions names.

Each boundary condition can be expressed in terms of spline coefficients as follows:

Bc1	
Lines	The line, i, where the condition is applied
Parameters	$\left[\alpha_{j-1}^i \quad \alpha_j^i \quad \alpha_{j+1}^i\right]$
Transf. coeff.	$\left[\frac{1}{6} \quad \frac{2}{3} \quad \frac{1}{6}\right]$

Table 2: Boundary conditions in displacements.

Bc2				
Lines	Line 1	Line 2	Line 3	Line 4
Parameters	$\left[\alpha_{j-1}^{1} \quad \alpha_{j}^{1} \quad \alpha_{j+1}^{1}\right]$	$\left[\alpha_{j-1}^{2} \quad \alpha_{j}^{2} \quad \alpha_{j+1}^{2}\right]$	$\left[\alpha_{j-1}^{3} \quad \alpha_{j}^{3} \quad \alpha_{j+1}^{3}\right]$	$\left[\alpha_{j-1}^{4} \quad \alpha_{j}^{4} \quad \alpha_{j+1}^{4}\right]$
Transf. coeff.	$L_1'(\xi_i)\cdot\left[\frac{1}{6} \quad \frac{2}{3} \quad \frac{1}{6}\right]$	$L_2'(\xi_i)\cdot\left[\frac{1}{6} \quad \frac{2}{3} \quad \frac{1}{6}\right]$	$L_3'(\xi_i)\cdot\left[\frac{1}{6} \quad \frac{2}{3} \quad \frac{1}{6}\right]$	$L_4'(\xi_i)\cdot\left[\frac{1}{6} \quad \frac{2}{3} \quad \frac{1}{6}\right]$

Table 3: Boundary conditions in ξ-derivative.

Bc3	
Lines	The line, i, where the condition is applied
Parameters	$\left[\alpha_{j-1}^{i} \quad \alpha_{j}^{i} \quad \alpha_{j+1}^{i}\right]$
Transf. coeff.	$\left[-\frac{1}{2} \quad 0 \quad \frac{1}{2}\right]$

Table 4: Boundary conditions in η-derivative.

Bc4				
Lines	Line 1	Line 2	Line 3	Line 4
Par.	$\left[\alpha_{j-1}^{1} \quad \alpha_{j}^{1} \quad \alpha_{j+1}^{1}\right]$	$\left[\alpha_{j-1}^{2} \quad \alpha_{j}^{2} \quad \alpha_{j+1}^{2}\right]$	$\left[\alpha_{j-1}^{3} \quad \alpha_{j}^{3} \quad \alpha_{j+1}^{3}\right]$	$\left[\alpha_{j-1}^{4} \quad \alpha_{j}^{4} \quad \alpha_{j+1}^{4}\right]$
Tr. coeff.	$\frac{\partial\xi}{\partial x}L_1'(\xi_i)\cdot\left[\frac{1}{6} \quad \frac{2}{3} \quad \frac{1}{6}\right]$ + $\delta_{1i}\frac{\partial\eta}{\partial x}\left[-\frac{1}{2} \quad 0 \quad \frac{1}{2}\right]$	$\frac{\partial\xi}{\partial x}L_2'(\xi_i)\cdot\left[\frac{1}{6} \quad \frac{2}{3} \quad \frac{1}{6}\right]$ + $\delta_{2i}\frac{\partial\eta}{\partial x}\left[-\frac{1}{2} \quad 0 \quad \frac{1}{2}\right]$	$\frac{\partial\xi}{\partial x}L_3'(\xi_i)\cdot\left[\frac{1}{6} \quad \frac{2}{3} \quad \frac{1}{6}\right]$ + $\delta_{3i}\frac{\partial\eta}{\partial x}\left[-\frac{1}{2} \quad 0 \quad \frac{1}{2}\right]$	$\frac{\partial\xi}{\partial x}L_4'(\xi_i)\cdot\left[\frac{1}{6} \quad \frac{2}{3} \quad \frac{1}{6}\right]$ + $\delta_{4i}\frac{\partial\eta}{\partial x}\left[-\frac{1}{2} \quad 0 \quad \frac{1}{2}\right]$

Table 5: Boundary conditions in x-derivative.

Bc5				
Lines	Line 1	Line 2	Line 3	Line 4
Par.	$\left[\alpha_{j-1}^1 \quad \alpha_j^1 \quad \alpha_{j+1}^1\right]$	$\left[\alpha_{j-1}^2 \quad \alpha_j^2 \quad \alpha_{j+1}^2\right]$	$\left[\alpha_{j-1}^3 \quad \alpha_j^3 \quad \alpha_{j+1}^3\right]$	$\left[\alpha_{j-1}^4 \quad \alpha_j^4 \quad \alpha_{j+1}^4\right]$
Tr. coeff.	$\frac{\partial\xi}{\partial y}L_1'(\xi_i)\cdot\left[\frac{1}{6} \quad \frac{2}{3} \quad \frac{1}{6}\right]$ + $\delta_{1i}\frac{\partial\eta}{\partial y}\left[-\frac{1}{2} \quad 0 \quad \frac{1}{2}\right]$	$\frac{\partial\xi}{\partial y}L_2'(\xi_i)\cdot\left[\frac{1}{6} \quad \frac{2}{3} \quad \frac{1}{6}\right]$ + $\delta_{2i}\frac{\partial\eta}{\partial y}\left[-\frac{1}{2} \quad 0 \quad \frac{1}{2}\right]$	$\frac{\partial\xi}{\partial y}L_3'(\xi_i)\cdot\left[\frac{1}{6} \quad \frac{2}{3} \quad \frac{1}{6}\right]$ + $\delta_{3i}\frac{\partial\eta}{\partial y}\left[-\frac{1}{2} \quad 0 \quad \frac{1}{2}\right]$	$\frac{\partial\xi}{\partial y}L_4'(\xi_i)\cdot\left[\frac{1}{6} \quad \frac{2}{3} \quad \frac{1}{6}\right]$ + $\delta_{4i}\frac{\partial\eta}{\partial y}\left[-\frac{1}{2} \quad 0 \quad \frac{1}{2}\right]$

Table 6: Boundary conditions in y-derivative.

In table 5 and 6,

$$\delta_{lm} = \begin{cases} 1 \text{ if } l = m \\ 0 \text{ if } l \neq m \end{cases} \qquad \textbf{Eq. 74}$$

The values assumed by the derivatives of the shape functions are listed in table 7:

	i=1	**i=2**	**i=3**	**i=4**
$L_1'(\xi_i)$	$-\frac{11}{4}$	$-\frac{1}{2}$	$\frac{1}{4}$	$-\frac{1}{2}$
$L_2'(\xi_i)$	$\frac{9}{2}$	$-\frac{3}{4}$	$-\frac{3}{2}$	$\frac{9}{4}$
$L_3'(\xi_i)$	$-\frac{9}{4}$	$\frac{3}{2}$	$\frac{3}{4}$	$-\frac{9}{2}$
$L_4'(\xi_i)$	$\frac{1}{2}$	$-\frac{1}{4}$	$\frac{1}{2}$	$\frac{11}{4}$

Table 7: Values of the first derivatives of the transverse shape functions in correspondence of the nodal lines.

From tables 2-6 the transformation matrix, **T**, can be constructed in such a way that,

$$\mathbf{T}\cdot\boldsymbol{\alpha} = \mathbf{a} \qquad \textbf{Eq. 75}$$

where the vector **a** is the transformed vector containing the desired combination of spline and physical coefficients. The values and the position of the coefficients of the row of **T** corresponding to a transformed physical coefficient are specified by the third and the second line, respectively, of the desired table (Tables 2 – 6), while the remaining components will be identically equal to zero.

From Eq. 48 and Eq. 49 it is possible to derive the conversion between the stiffness matrix, $\mathbf{K}_s$, originally defined in spline coefficients, $\boldsymbol{\alpha}$, to the stiffness matrix $\tilde{\mathbf{K}}_s$ referring to the physical components, **a**, as

$$\tilde{\mathbf{K}}_s = \mathbf{T}^{-T} \cdot \mathbf{K}_s \cdot \mathbf{T}^{-1} \qquad \text{Eq. 76}$$

Similarly, from Eq. 50 and Eq. 51, the conversion between the load vector $\mathbf{v}_s$ and one referring to physical coefficients, $\tilde{\mathbf{v}}_s$, is

$$\tilde{\mathbf{v}}_s = \mathbf{T}^{-T} \cdot \mathbf{v}_s \qquad \text{Eq. 77}$$

The transformation matrix **T** will then contain the conversions needed for the longitudinal assembly of adjoining strips and all the required changes to impose the boundary conditions. The method of converting spline coefficients to physical coefficients was termed the "transformation method" by Leung and Au (1990).

For the sake of simplicity, the transformation matrix **T** has been here presented and applied at strip level, while in the computer program developed it is applied to the assembly of strips longitudinally interconnected and traditionally assembled transversely.

It should be noted that the choice of the spline coefficients to transform in order to perform the longitudinal assembly and ensuring a sufficient degree of continuity is not arbitrary. While it is clearly necessary to transform the second and the last spline coefficients of each nodal line into displacement coefficients to ensure continuity in displacements, by choosing to transform the first and the second last spline coefficient for each nodal line into the derivative of the displacement in y, $\frac{\partial \delta}{\partial y}$, the continuity in rotation, $\frac{\partial \delta}{\partial x}$, is, in fact, also ensured. This can be proved by showing how the derivative of the general displacement in x, $\frac{\partial \delta}{\partial x}$, evaluated at the ends of a nodal line, can be expressed as a linear combination of the displacement δ and its derivatives in y, $\frac{\partial \delta}{\partial y}$, evaluated at the ends of each nodal line of the strip.

To prove this we may develop the calculations regarding the displacement field and its derivatives at the starting longitudinal edge of the strip ($\eta = 0$).

Introducing,

$$u_1 = u(-1,0)$$
$$u_2 = u(-1/3,0)$$
$$u_3 = u(1/3,0)$$
$$u_4 = u(1,0)$$

Eq. 78

the displacement field corresponding to the nodal lines becomes:

$$u_1 = \sum_{i=1}^{4}\sum_{j=-1}^{1} L_i(-1)\cdot\phi_j(0)\,\alpha_j^i = \sum_{j=-1}^{1}\phi_j(0)\,\alpha_j^1 = \begin{bmatrix}\frac{1}{6} & \frac{2}{3} & \frac{1}{6}\end{bmatrix}\begin{bmatrix}\alpha_{-1}^1\\ \alpha_0^1\\ \alpha_1^1\end{bmatrix} \quad \textbf{Eq. 79}$$

$$u_2 = \sum_{i=1}^{4}\sum_{j=-1}^{1} L_i(-1/3)\cdot\phi_j(0)\,\alpha_j^i = \sum_{j=-1}^{1}\phi_j(0)\,\alpha_j^2 = \begin{bmatrix}\frac{1}{6} & \frac{2}{3} & \frac{1}{6}\end{bmatrix}\begin{bmatrix}\alpha_{-1}^2\\ \alpha_0^2\\ \alpha_1^2\end{bmatrix} \quad \textbf{Eq. 80}$$

$$u_3 = \sum_{i=1}^{4}\sum_{j=-1}^{1} L_i(1/3)\cdot\phi_j(0)\,\alpha_j^i = \sum_{j=-1}^{1}\phi_j(0)\,\alpha_j^3 = \begin{bmatrix}\frac{1}{6} & \frac{2}{3} & \frac{1}{6}\end{bmatrix}\begin{bmatrix}\alpha_{-1}^3\\ \alpha_0^3\\ \alpha_1^3\end{bmatrix} \quad \textbf{Eq. 81}$$

$$u_4 = \sum_{i=1}^{4}\sum_{j=-1}^{1} L_i(1)\cdot\phi_j(0)\,\alpha_j^i = \sum_{j=-1}^{1}\phi_j(0)\,\alpha_j^4 = \begin{bmatrix}\frac{1}{6} & \frac{2}{3} & \frac{1}{6}\end{bmatrix}\begin{bmatrix}\alpha_{-1}^4\\ \alpha_0^4\\ \alpha_1^4\end{bmatrix} \quad \textbf{Eq. 82}$$

Introducing now for simplicity,

$$\tilde{u}' = u'(-1,0)_1 = \sum_{i=1}^{4}\sum_{j=-1}^{1} L_i(-1)\cdot\phi_j'(0)\,\alpha_j^i = \sum_{j=-1}^{1}\phi_j'(0)\,\alpha_j^1 = \begin{bmatrix}-\frac{1}{2} & 0 & \frac{1}{2}\end{bmatrix}\begin{bmatrix}\alpha_{-1}^1\\ \alpha_0^1\\ \alpha_1^1\end{bmatrix} \quad \textbf{Eq. 83}$$

$$\tilde{u}_2' = u'\left(-\frac{1}{3},0\right) = \sum_{i=1}^{4}\sum_{j=-1}^{1} L_i(-1/3)\cdot\phi_j'(0)\,\alpha_j^i = \sum_{j=-1}^{1}\phi_j'(0)\,\alpha_j^2 = \begin{bmatrix}-\frac{1}{2} & 0 & \frac{1}{2}\end{bmatrix}\begin{bmatrix}\alpha_{-1}^2\\ \alpha_0^2\\ \alpha_1^2\end{bmatrix} \quad \textbf{Eq. 84}$$

$$\tilde{u}_3' = u'\left(\frac{1}{3},0\right) = \sum_{i=1}^{4}\sum_{j=-1}^{1} L_i(1/3)\cdot\phi_j'(0)\,\alpha_j^i = \sum_{j=-1}^{1}\phi_j'(0)\,\alpha_j^3 = \begin{bmatrix}-\frac{1}{2} & 0 & \frac{1}{2}\end{bmatrix}\begin{bmatrix}\alpha_{-1}^3\\ \alpha_0^3\\ \alpha_1^3\end{bmatrix} \quad \textbf{Eq. 85}$$

$$\tilde{u}_4' = u'(1,0) = \sum_{i=1}^{4}\sum_{j=-1}^{1} L_i(1)\cdot\phi_j'(0)\,\alpha_j^i = \sum_{j=-1}^{1}\phi_j'(0)\,\alpha_j^4 = \begin{bmatrix}-\frac{1}{2} & 0 & \frac{1}{2}\end{bmatrix}\begin{bmatrix}\alpha_{-1}^4\\ \alpha_0^4\\ \alpha_1^4\end{bmatrix} \quad \textbf{Eq. 86}$$

we may also express the derivative of the displacement in the global x-coordinate:

$$\frac{\partial u_1}{\partial x} = \frac{\partial u_1}{\partial \xi}\frac{\partial \xi}{\partial x} + \frac{\partial u_1}{\partial \eta}\frac{\partial \eta}{\partial x} = \left(\sum_{i=1}^{4}\sum_{j=-1}^{1} L_i'(-1)\cdot\phi_j(0)\,\alpha_j^i\right)\frac{\partial \xi}{\partial x} + \left(\sum_{i=1}^{4}\sum_{j=-1}^{1} L_i(-1)\cdot\phi_j'(0)\,\alpha_j^i\right)\frac{\partial \eta}{\partial x}$$
$$= \left(L_1'(-1)\cdot u_1 + L_2'(-1)\cdot u_2 + L_3'(-1)\cdot u_3 + L_4'(-1)\cdot u_4\right)\frac{\partial \xi}{\partial x} + \tilde{u}_1'\frac{\partial \eta}{\partial x} \qquad \textbf{Eq. 87}$$

and, in the same way, the derivative of the displacement in the global y-coordinate:

$$\frac{\partial u_1}{\partial y} = \frac{\partial u_1}{\partial \xi}\frac{\partial \xi}{\partial y} + \frac{\partial u_1}{\partial \eta}\frac{\partial \eta}{\partial y} = \left(\sum_{i=1}^{4}\sum_{j=-1}^{1} L_i'(-1)\cdot\phi_j(0)\,\alpha_j^i\right)\frac{\partial \xi}{\partial y} + \left(\sum_{i=1}^{4}\sum_{j=-1}^{1} L_i(-1)\cdot\phi_j'(0)\,\alpha_j^i\right)\frac{\partial \eta}{\partial y}$$
$$= \left(L_1'(-1)\cdot u_1 + L_2'(-1)\cdot u_2 + L_3'(-1)\cdot u_3 + L_4'(-1)\cdot u_4\right)\frac{\partial \xi}{\partial y} + \tilde{u}_1'\frac{\partial \eta}{\partial y} \qquad \textbf{Eq. 88}$$

It is also convenient to introduce,

$$a = \frac{\partial \xi}{\partial x} \qquad b = \frac{\partial \eta}{\partial x} \qquad c = \frac{\partial \xi}{\partial y} \qquad d = \frac{\partial \eta}{\partial y} \qquad \textbf{Eq. 89}$$

Comparing then Eq. 88 with Eq. 79 - Eq. 82 and Eq. 87 it follows that,

$$\frac{\partial u_1}{\partial y} = \frac{d}{b}\frac{\partial u_1}{\partial x} + \left(c - \frac{ad}{b}\right)\left(\frac{u_1}{L_1'(-1)} + \frac{u_2}{L_2'(-1)} + \frac{u_3}{L_3'(-1)} + \frac{u_4}{L_4'(-1)}\right) \qquad \textbf{Eq. 90}$$

Similarly, evaluating Eq. 82 at the other nodal lines we obtain,

$$\frac{\partial u_2}{\partial y} = \frac{d}{b}\frac{\partial u_2}{\partial x} + \left(c - \frac{ad}{b}\right)\left(\frac{u_1}{L_1'(-1/3)} + \frac{u_2}{L_2'(-1/3)} + \frac{u_3}{L_3'(-1/3)} + \frac{u_4}{L_4'(-1/3)}\right) \qquad \textbf{Eq. 91}$$

$$\frac{\partial u_3}{\partial y} = \frac{d}{b}\frac{\partial u_3}{\partial x} + \left(c - \frac{ad}{b}\right)\left(\frac{u_1}{L_1'(1/3)} + \frac{u_2}{L_2'(1/3)} + \frac{u_3}{L_3'(1/3)} + \frac{u_4}{L_4'(1/3)}\right) \qquad \textbf{Eq. 92}$$

$$\frac{\partial u_4}{\partial y} = \frac{d}{b}\frac{\partial u_4}{\partial x} + \left(c - \frac{ad}{b}\right)\left(\frac{u_1}{L_1'(1)} + \frac{u_2}{L_2'(1)} + \frac{u_3}{L_3'(1)} + \frac{u_4}{L_4'(1)}\right) \qquad \textbf{Eq. 93}$$

The linear dependence between the physical components $\frac{\partial u}{\partial x}$ and $\frac{\partial u}{\partial y}$ is hence proved.

As a concluding remark, it is highlighted that the choice of transforming the spline coefficients into derivatives in y rather than in x (i.e. applying the Bc5-condition rather than Bc4) is due to the fact that, for non-distorted rectangular strips, the derivative $\frac{\partial \eta}{\partial x}$ in table 5 vanishes. In that case, the Bc4-condition reduces to a linear combination of Bc1-conditions in the four nodal lines of a

strip. This is not the case for Bc5-condition where, while the derivative $\frac{\partial \xi}{\partial y}$ vanishes in rectangular strips, the other component, $\frac{\partial \eta}{\partial y}$, never vanishes thus produces linearly independent rows in the transformation matrix **T**.

4- Examples

The present formulation has been coded in a fortran computer program to demonstrate its accuracy and reliability. Three examples are here listed where results obtained with the present formulation are tested against exact theoretical solutions and numerical results obtained utilising the commercial package Abaqus (ABAQUS 2003).
The following examples concern thin plates in mono-dimensional traction containing cut-outs of different shapes. In particular, the cases of a circular, rectangular and key-shaped hole are presented.

4.1- Circular Hole

The problem of an infinite elastic plate in tension with a circular hole has been analysed. An exact linear elastic solution is available for this problem (Timoshenko and Goodier 1970). The geometry of the problem is shown in Fig. 5.

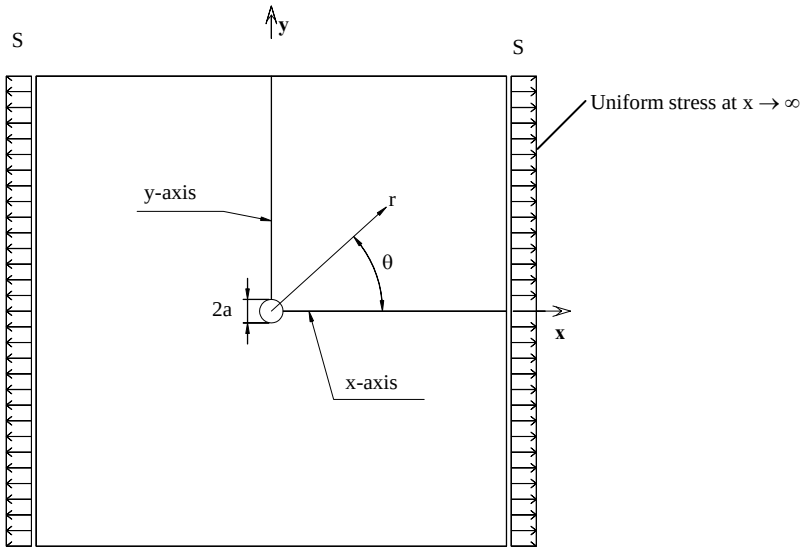

Fig. 5: Circular hole: geometry of the plate.

The solution is provided in terms of the polar coordinates, r and θ (Fig. 5) and is given by

$$\sigma_r = \frac{S}{2}\cdot\left(1-\frac{a^2}{r^2}\right)+\frac{S}{2}\cdot\left(1+\frac{3a^4}{r^4}-\frac{4a^2}{r^2}\right)\cdot\cos 2\theta \qquad \textbf{Eq. 94}$$

$$\sigma_\theta = \frac{S}{2}\cdot\left(1+\frac{a^2}{r^2}\right)-\frac{S}{2}\cdot\left(1+\frac{3a^4}{r^4}\right)\cdot\cos 2\theta \qquad \textbf{Eq. 95}$$

$$\tau_{r\theta} = -\frac{S}{2}\cdot\left(1-\frac{3a^4}{r^4}+\frac{2a^2}{r^2}\right)\cdot\sin 2\theta \qquad \textbf{Eq. 96}$$

which can be easily converted to global xy-coordinates as follows

$$\sigma_x = \sigma_r\cdot\cos^2\theta+\sigma_\theta\cdot\sin^2\theta-2\tau_{r\theta}\cdot\sin\theta\cos\theta \qquad \textbf{Eq. 97}$$

$$\sigma_y = \sigma_r\cdot\sin^2\theta+\sigma_\theta\cdot\cos^2\theta+2\tau_{r\theta}\cdot\sin\theta\cos\theta \qquad \textbf{Eq. 98}$$

$$\tau_{xy} = (\sigma_r-\sigma_\theta)\cdot\sin\theta\cos\theta+\tau_{r\theta}\cdot(\cos^2\theta-\sin^2\theta) \qquad \textbf{Eq. 99}$$

In the numerical analysis only half of the geometry was considered, taking advantage of the symmetry along the x-axis. Even though the exact solution applies to an infinite space, the numerical analysis has been performed on a finite linear elastic space of unity thickness, i.e.

$$\{(x,y):\quad x\in[-30,30],\qquad y\in[0,30]\} \qquad \textbf{Eq. 100}$$

The external forces applied to the boundaries (x = -30, y = 30 and x = 30) of the bi-dimensional sub-space defined by Eq. 100 have been derived from Eq. 97 to Eq. 99 taking the intensity (S) as the applied stress as 10^4.

Fig. 6 illustrates the mesh employed in the isoparametric spline finite strip analysis. The strips are running in the longitudinal y-direction while the principal traction is applied in the transverse x-direction. The reason for choosing this orientation is that the stress distribution (Eq. 97 to Eq. 99) along the edge y = 30 is more complex than along the edge corresponding to x = 30 even if of lesser intensity. The computer program developed interpolates the external forces applied in the transverse direction (ξ) with cubic polynomials, while only a linear interpolation is utilised for the external forces acting in the longitudinal direction (η). Furthermore, the symmetry boundary conditions can be applied along transverse edges (e.g. along the ξ-coordinate), while boundary conditions regarding transverse derivatives ($\frac{\partial\delta}{\partial\xi}, \frac{\partial\delta}{\partial x}, \frac{\partial\delta}{\partial y}$, i.e. Bc2, Bc4, Bc5) can only be applied node-wise but not enforced along the entire nodal line. It can be seen from tables 3, 5 and 6 that these boundary conditions involve the first derivative of the transverse shape functions, L_i'. Considering for example the

derivative with respect to the transverse natural coordinate, $\frac{\partial \delta}{\partial \xi}$, its value along the first longitudinal nodal line of the strip (i.e. $\xi = \xi_1 = -1$) can be expressed as

$$\frac{\partial \delta}{\partial \xi}(\xi_1, \eta) = \sum_{i=1}^{4} \sum_{j=-1}^{m_s+1} L_i'(\xi_1) \cdot \phi_j(\eta) \cdot \alpha_{ij}^{\delta} \qquad \textbf{Eq. 101}$$

From the second column of table 7 it can be observed that all of the transverse shape polynomials (L_i') attain non-zero values. The values of $\frac{\partial \delta}{\partial \xi}$ along a nodal line depend therefore not only on the spline coefficients along that line but also on the spline coefficients defined over the other nodal lines of the strip, i.e. on a total of 4(m+3) coefficients. It follows that it is not possible to impose a boundary condition along the entire longitudinal edge in terms of the m+3 nodes along that edge. This explains why only the symmetry along the x-axis has been exploited in the analysis.

Fig. 6 also illustrates the number of intermediate spline sections (m). The number of sections utilised in macro-sections 1 and 2 is such as their average length is almost the same. A macro-section is here an assembly of parallel strips of equal length. The macro-sections 1, 2 and 3 shown in Fig. 6 contain respectively 12, 14 and 14 strips transversally

Consistently with the model used for the finite strip analysis, the finite element model analysed with the commercial package Abaqus is shown in Fig. 7. An automatic adaptive mesh has been employed.

The solutions obtained with the different numerical models as well as the one derived from the exact solution are compared along the two symmetry axes, shown as the x-axis and y-axis in Fig. 5. The comparison of stress components (σ_x, σ_y) referring to the global directions is illustrated in Fig. 8 and Fig. 9.

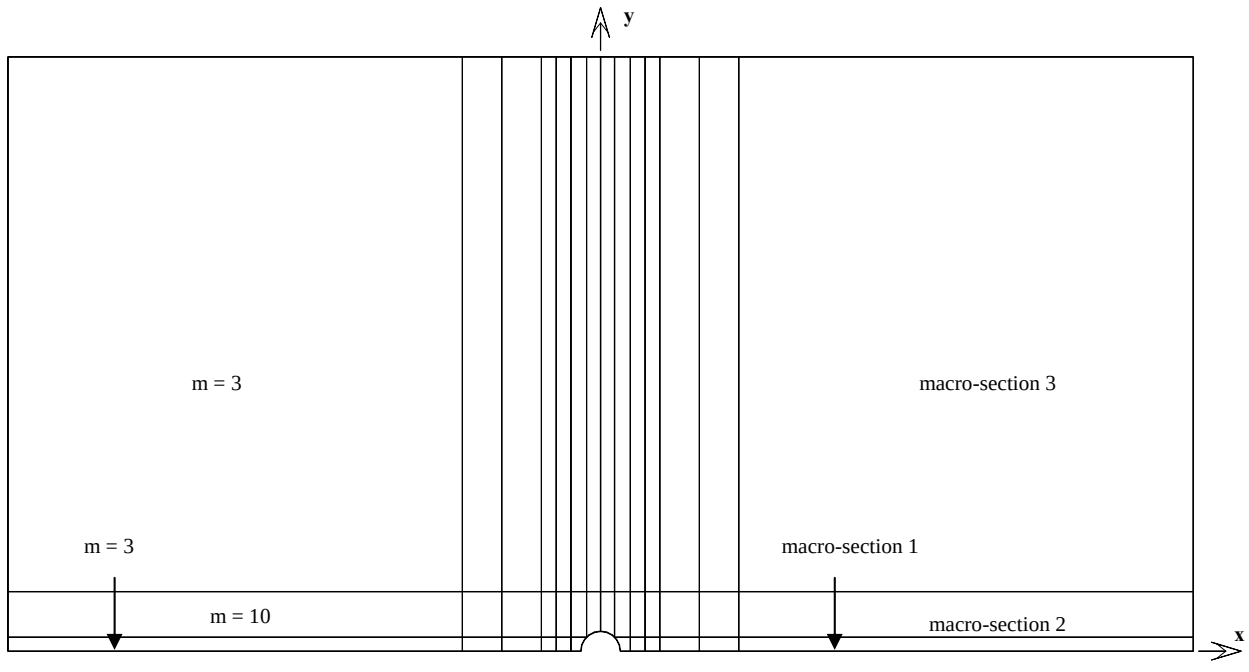

Fig. 6: Circular hole: finite strip mesh.

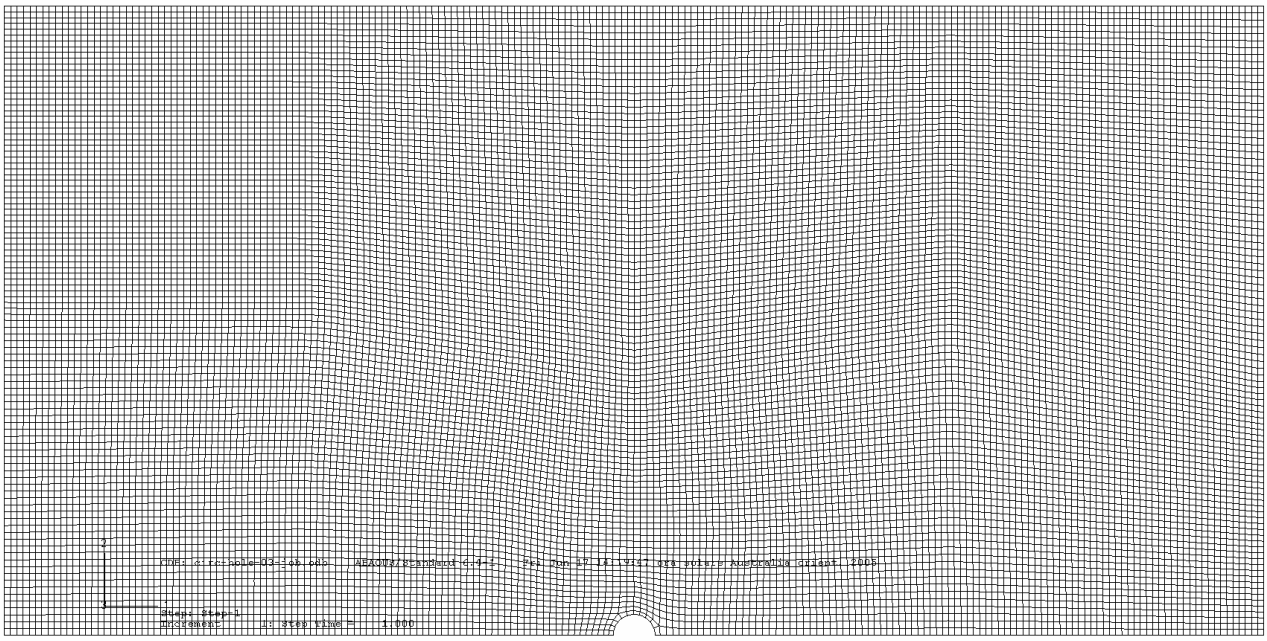

Fig. 7: Circular hole: finite element mesh.

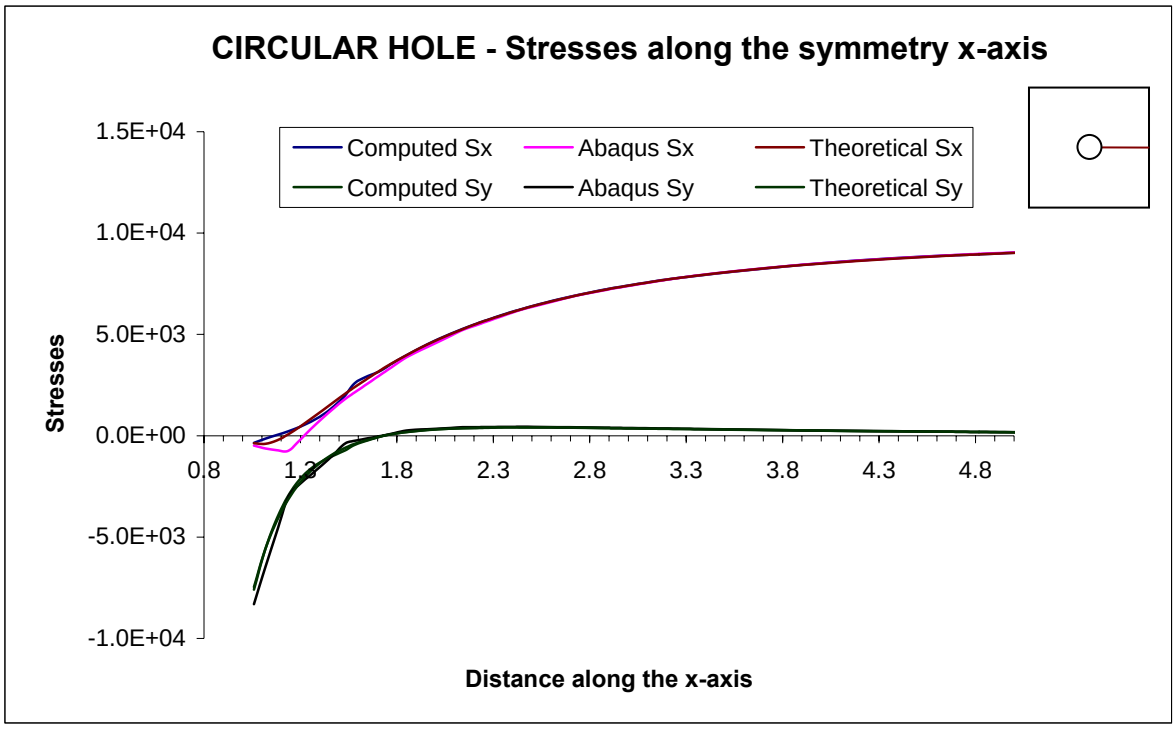

Fig. 8: Circular hole: stress comparison along the symmetry x-axis.

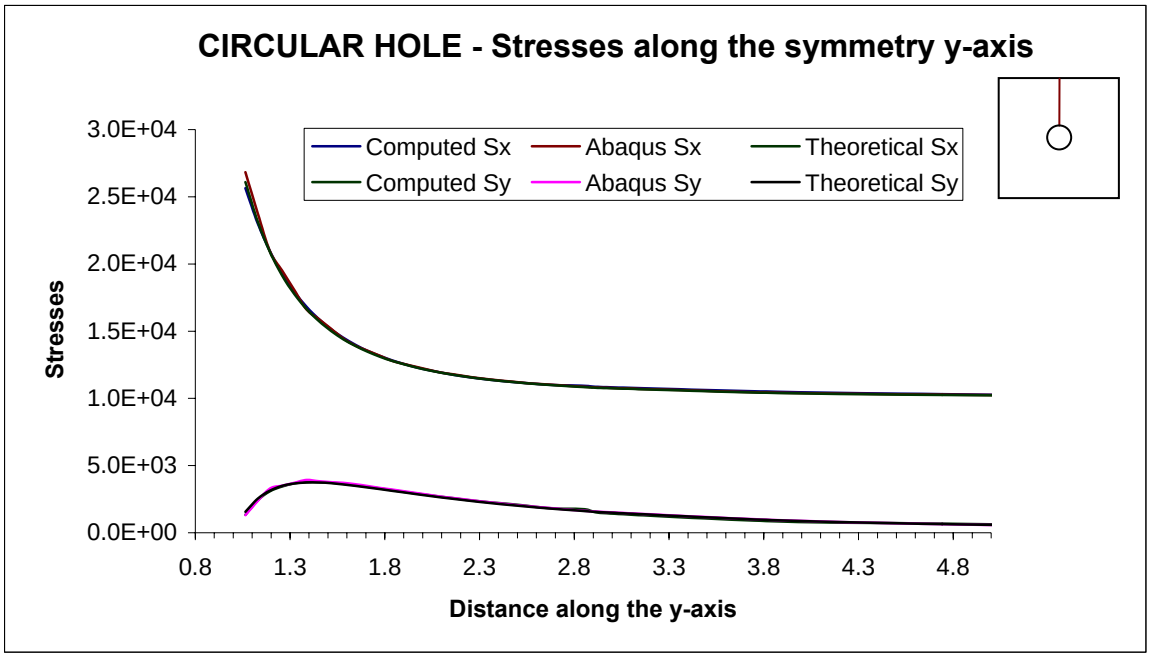

Fig. 9: Circular hole: stress comparison along the symmetry y-axis.

The general agreement between the two sets of results may be observed. It may be noted how, despite the relatively coarse mesh utilised in the spline finite strip method, that the solution obtained is very close to the exact one. The finite element curve is obtained by means of quadratic 8 node elements. It is slightly less accurate then the spline finite strip method. Better results could be obtained by refining the mesh in the area around the circular hole. In terms of computational effort it is noticed that to achieve the same accuracy in finite element analysis the number of degrees of freedom required is about two orders of magnitude larger than the number of degrees of freedom used in the finite strip analysis.

A normalized error trend is presented in the following. In Fig. 10 and Fig. 11 the difference between the stresses calculated by the finite strip method and the exact solution is normalised with regard to the maximum stress component along the reference axis. In Fig. 12 and Fig. 13 the relative error is weighted with regard to the Von Mises stress computed at that specific point. In both situations it is possible to observe how the error is relatively small and that its maximum values are located in the areas where that particular stress component intensity is small. The larger errors generally refer to the x-axis. One possible reason is that along that direction the solution accuracy is determined by the transverse shape functions and is strongly related to the width of the strips which is actually two or three times the length of the longitudinal sections utilised in this example.

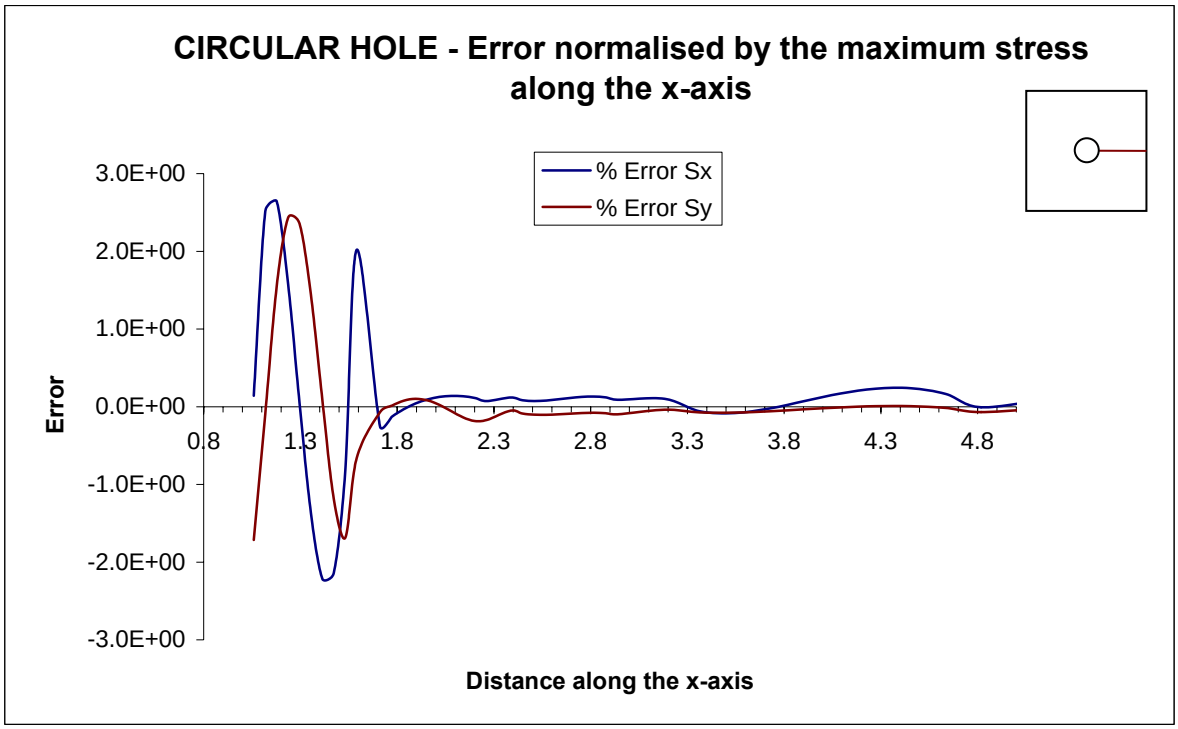

Fig. 10: Circular hole: error normalised with respect to the maximum correspondent stress along the x-axis.

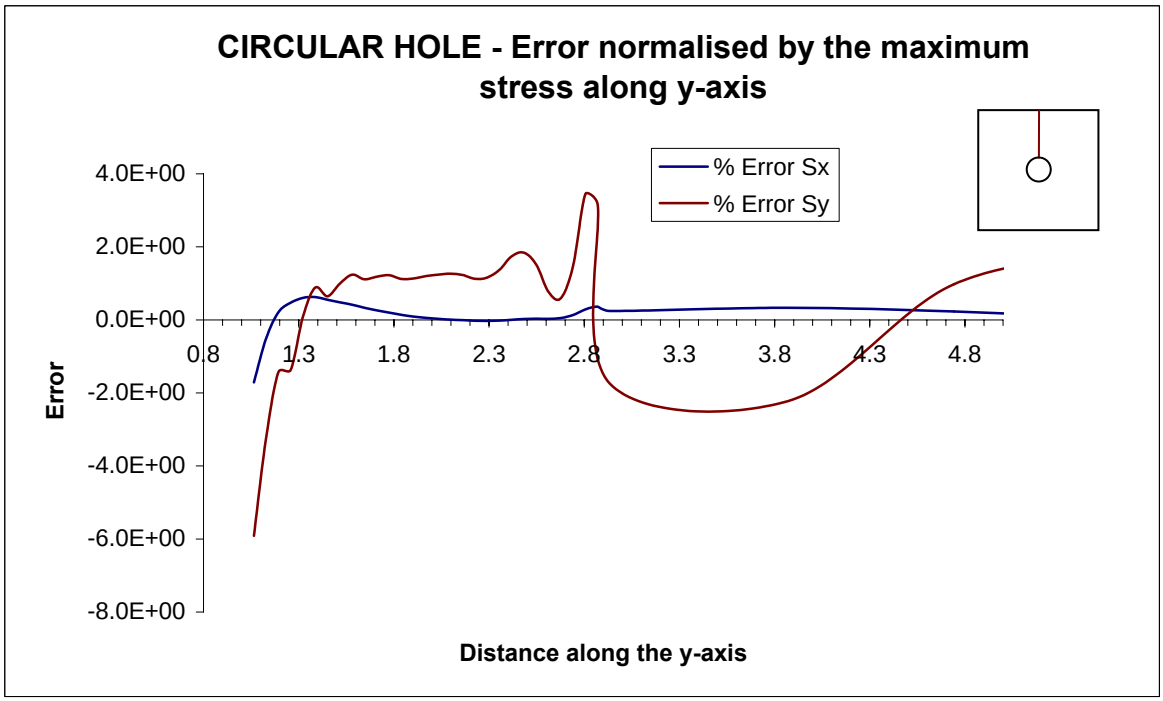

Fig. 11: Circular hole: error normalised with respect to the maximum correspondent stress along the y-axis.

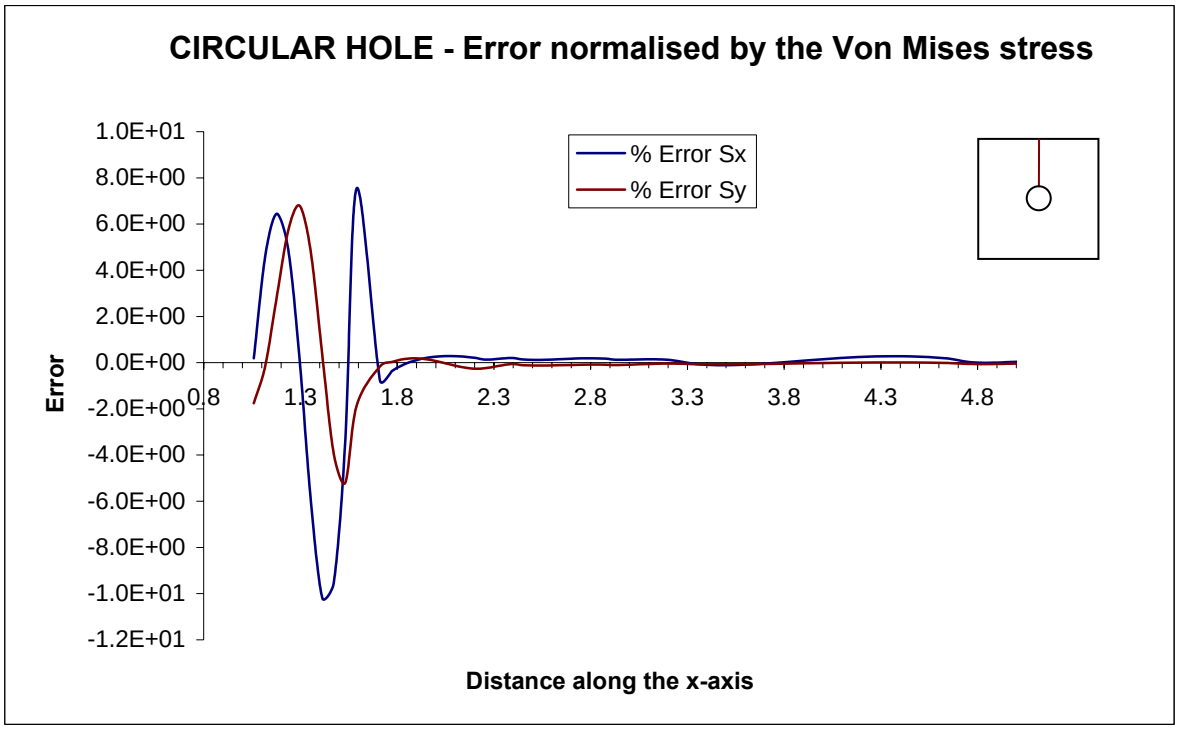

Fig. 12: Circular hole: error along the x-axis normalised with respect to the Von Mises stress.

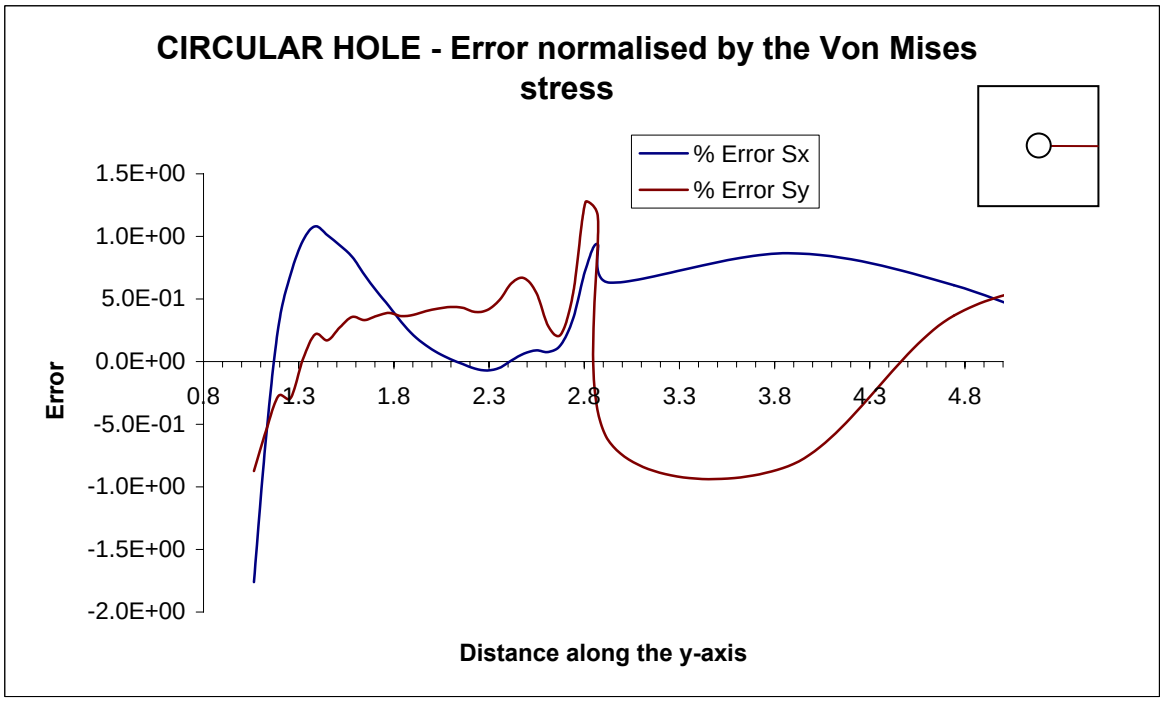

Fig. 13: Circular hole: error along the y-axis normalised with respect to the Von Mises stress.

4.2- Rectangular Hole

Similarly to the case of the circular hole, the results of the analysis of a plate containing a rectangular cut-out are now presented. This particular example has been chosen to test the accuracy of the proposed method at singularity points, i.e. the sharp corners of a hole.

The geometry of the square plate with a rectangular hole at the centre is shown in Fig. 14. The dimensions of the plate and hole are expressed in terms of an arbitrary unit dimension "a". The side of the plate is assumed equal to 20a while its thickness is 1a. The major axis of the rectangular cut-out is parallel to the y-axis and the dimensions of the hole are 2a x 4a.

The system of external forces is a uniform traction of intensity 10^4 in the londitudinal y-direction. The symmetry along the x-axis has been exploited. Only half of the plate has hence been analysed. The results obtained with the isoparametric cubic spline finite strip method have been tested against the results obtained with Abaqus and are compared along four reference axes, namely x-axis-1, x-axis-2, y-axis-1 and y-axis-2, as shown in Fig. 14.

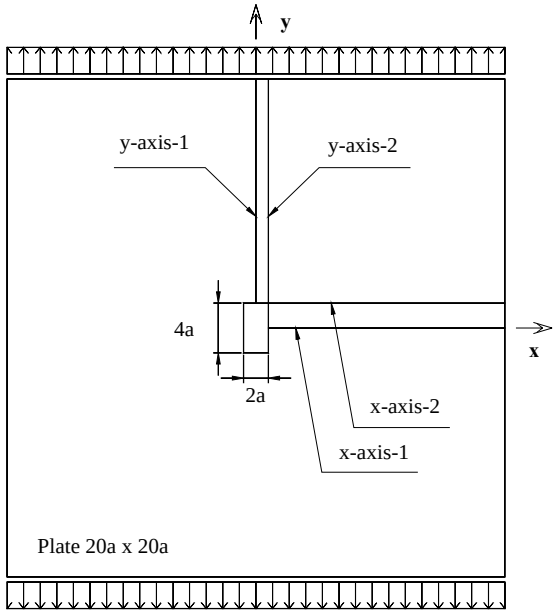

Fig. 14: Geometry of the rectangular hole problem.

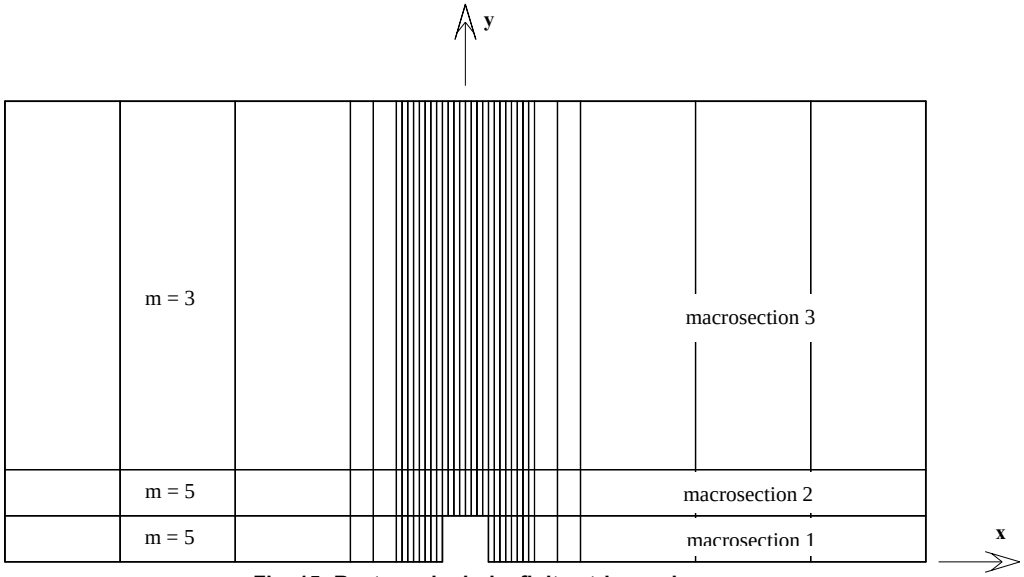

Fig. 15: Rectangular hole: finite strip mesh.

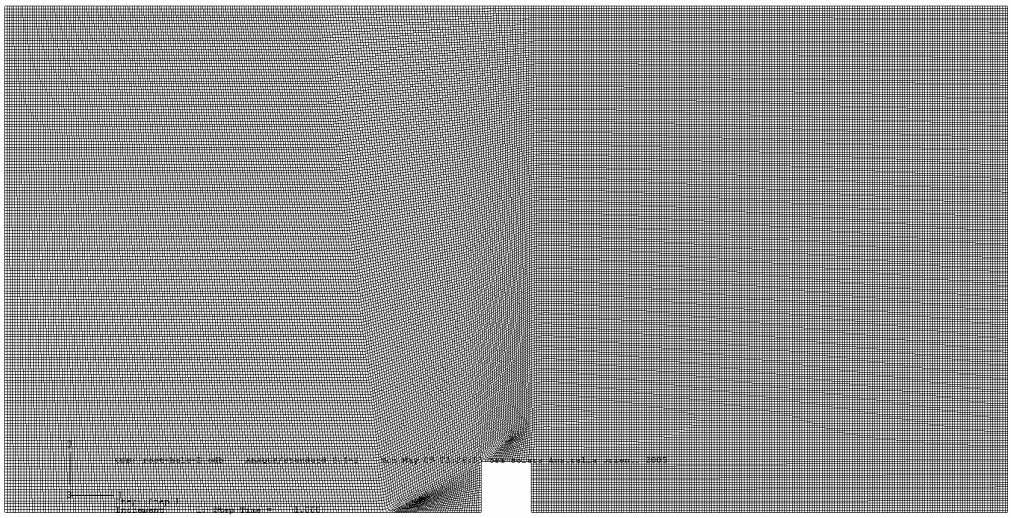

Fig. 16: Rectangular hole: finite element mesh.

Fig. 15 and Fig. 16 show the mesh employed for the finite strip analysis and the finite element analysis respectively. There is no closed-form solution for this problem.

The solutions are compared in the graphs shown in Fig. 17 to Fig. 20. The graphs have been truncated at a distance of 10 units from the centre of the hole so as to focus on the region around the hole. It can be observed that the solutions differ only in the area immediately around the corner of the hole, while they are practically coincident elsewhere.

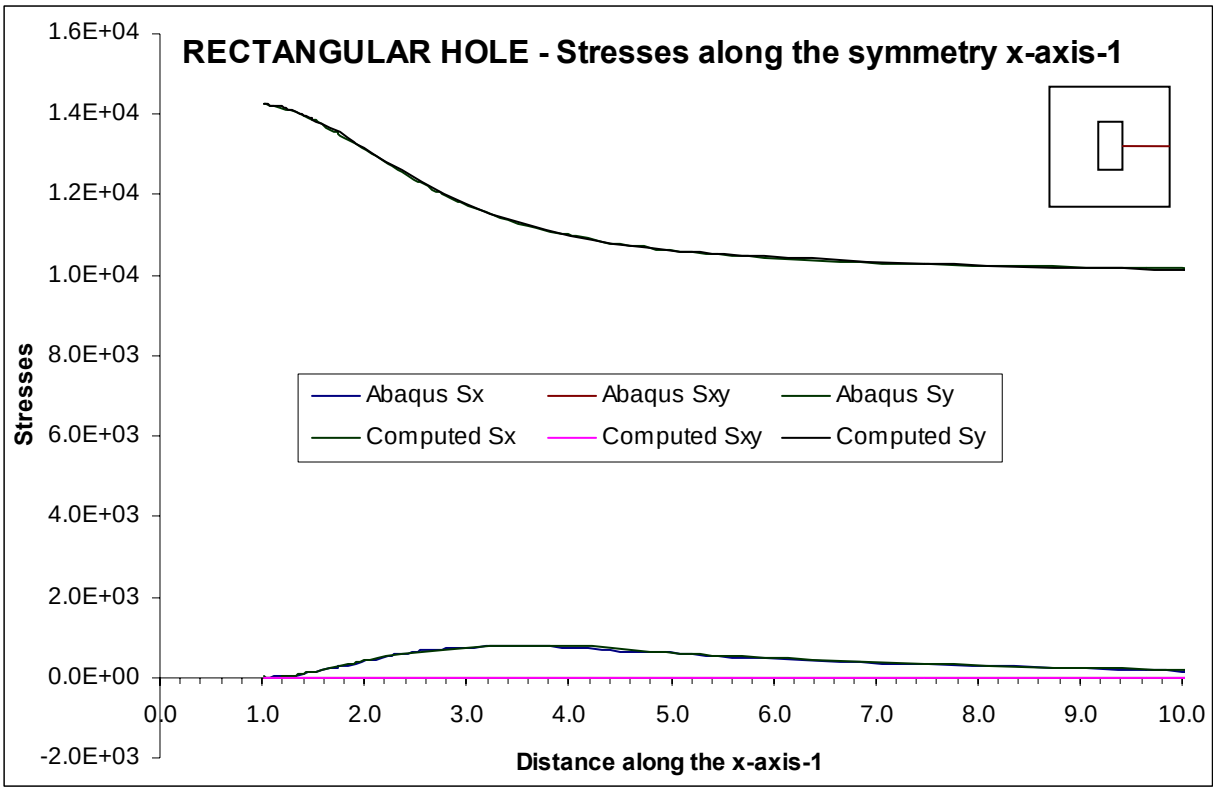

Fig. 17: Rectangular hole: stress distribution along the symmetry x-axis-1.

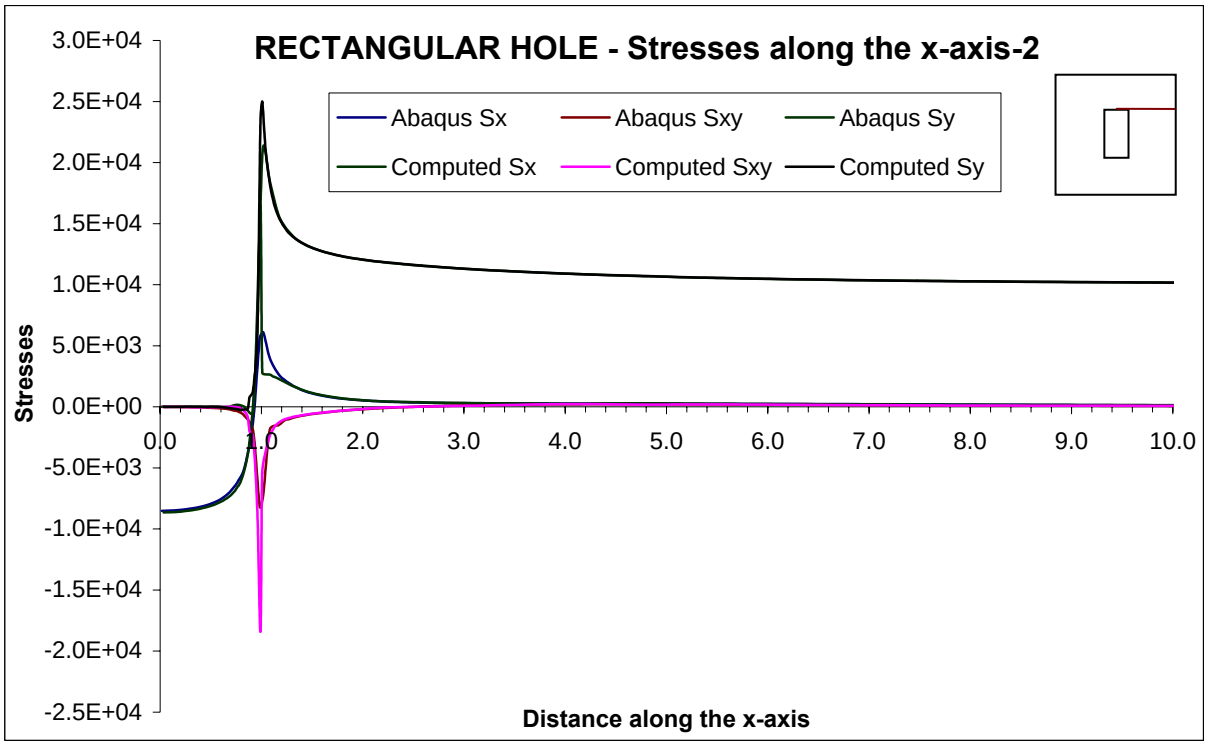

Fig. 18: Rectangular hole: stress distribution along the x-axis-2.

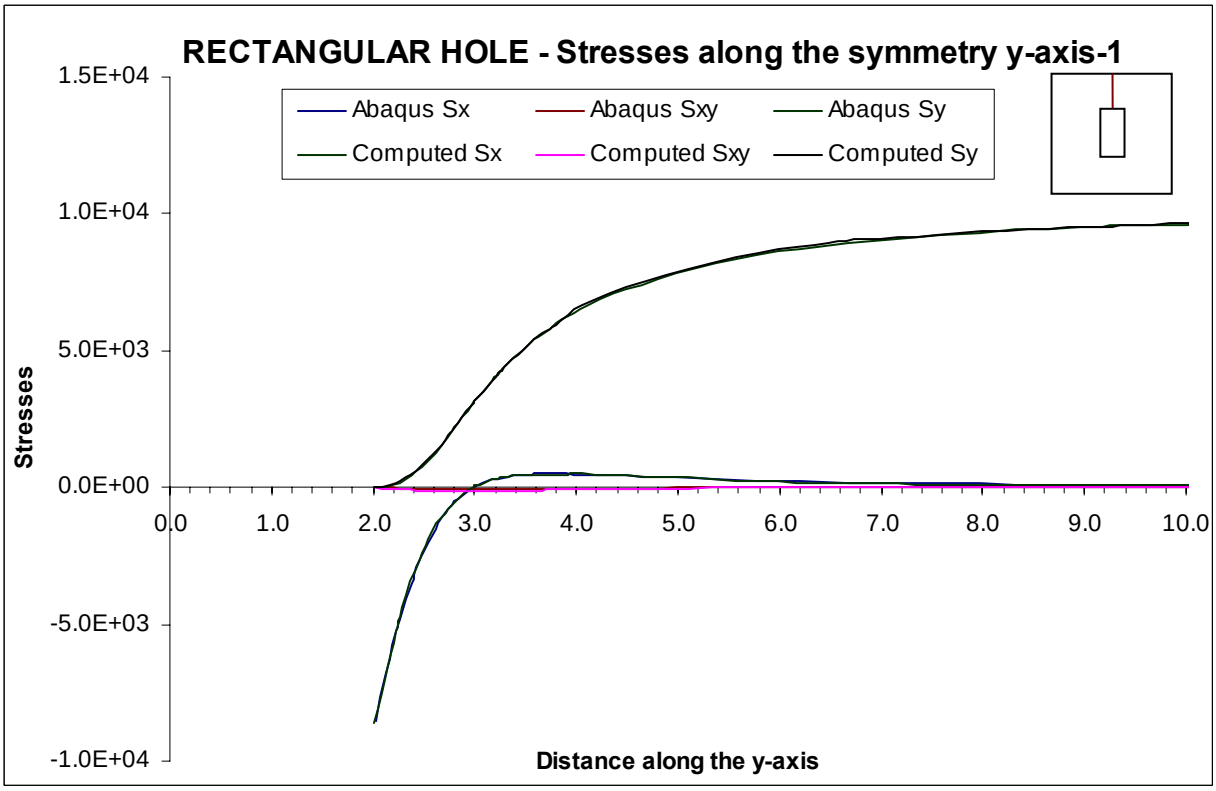

Fig. 19: Rectangular hole: stress distribution along the symmetry y-axis-1.

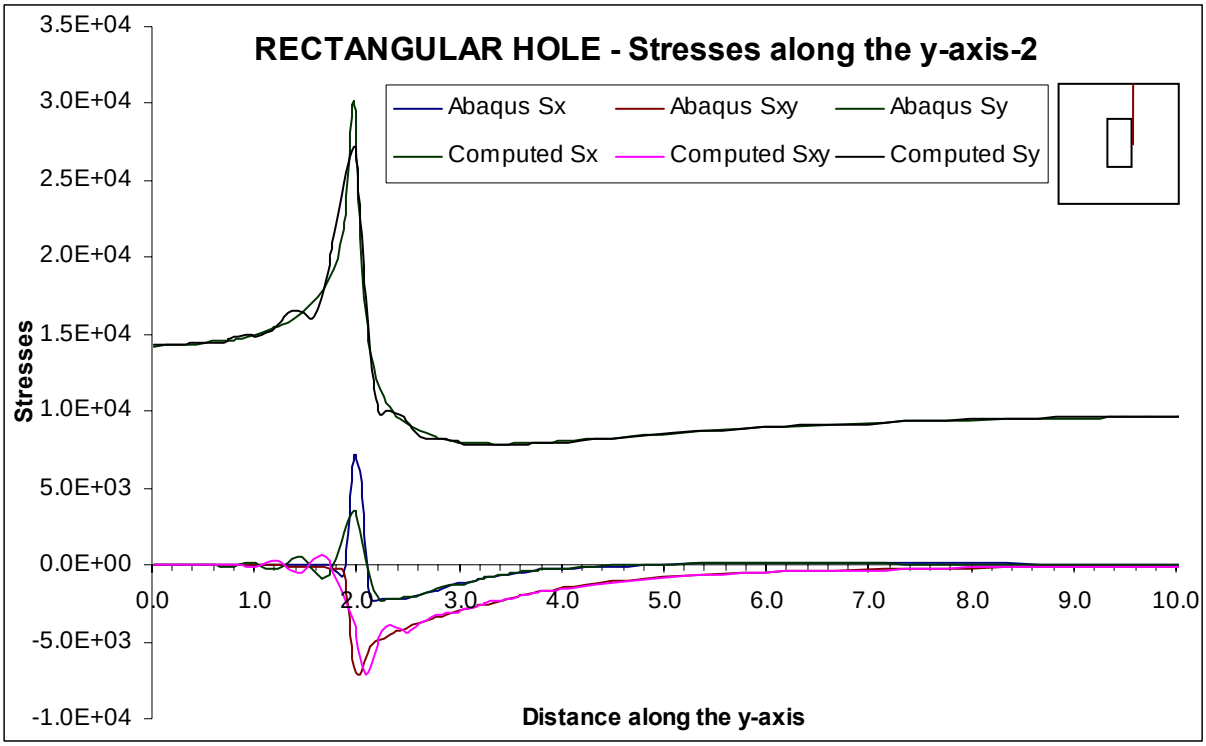

Fig. 20: Rectangular hole: stress distribution along the y-axis-2.

The general agreement of the results can be noted. In the graphs reproducing the behavior in the corner area with regard to the longitudinal y-direction (Fig. 20), an oscillatory response of the finite strip analysis is highlighted. In the comparison shown, the ratio between the finite element mesh size and the finite strip mesh size is approximately 8/20 in the x direction and 5/20 in the y direction (in the region of the corner). By increasing the number of longitudinal sections (m) the oscillatory behaviour is "squeezed" towards the corner of the cut-out and the spline finite strip curve approaches the finite element curve (except at the corner itself where the singularity of the point leads to increasing values of the stress when refining the mesh).
It is again remarked how a sufficient stress definition within the plate can be obtained with a relatively small number of strips, proving the efficiency of the present method.

4.3- Key-Shaped Hole

In addition to the two previous examples, a third one concerning a key-shaped cut-out is now presented. This configuration is often used in the industrial steel storage rack industry to provide an easy connection between beams and columns. The example combines the main features highlighted in the two previous examples. The geometry of the plate is shown in Fig. 21. The plate dimensions and its thickness are expressed in terms of an arbitrary unity dimension "a". The overall dimensions of the plate are 10a x 20a and its thickness has been assumed to be 1a. Consistent with the circular and the rectangular hole cases, the numerical analyses has been performed with both the

spline finite strip method and the finite element method (Abaqus). The different discretisations adopted are shown in Fig. 22 and Fig. 23. Also in this case, in adopting the Abaqus results as reference to assess the accuracy of the proposed method, a very fine mesh has been utilised.

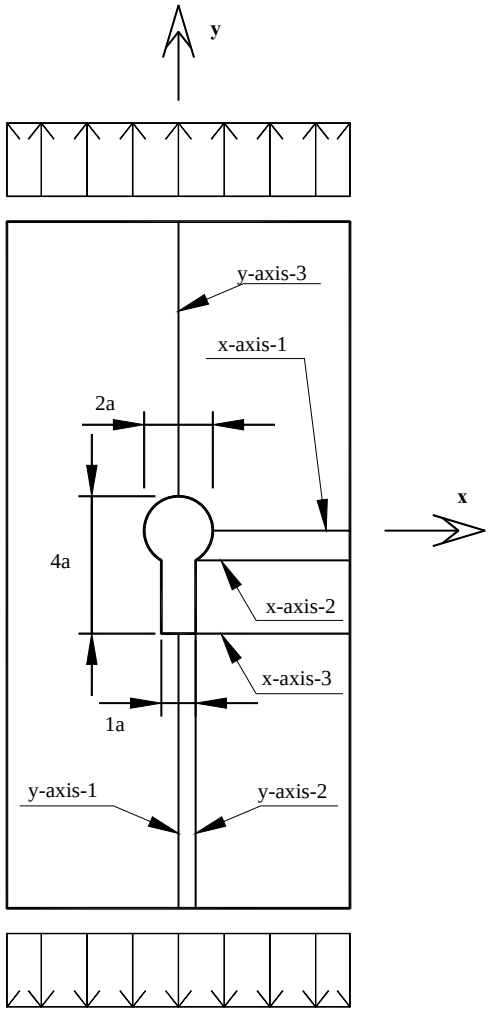

Fig. 21: Key-shaped hole: plate geometry.

The stress distributions along the six different reference axes shown in Fig. 21 are presented in Fig. 24 and Fig. 25. Compared to the previous examples, a higher stress concentration is found at the edge of the circular hole (compare Fig. 8 and Fig. 24). The oscillatory behaviour in the proximity of the singularity point at the corner of the hole is noticed again. In this example a much finer mesh is utilised for the spline finite strip analysis, resulting in a better agreement between the Abaqus and the computed curves and, furthermore, in a shift of the oscillatory part towards the corner of the hole (Fig. 28). An almost coincident stress distribution is recorded along the other axes (Fig. 25, Fig. 27 and Fig. 29)

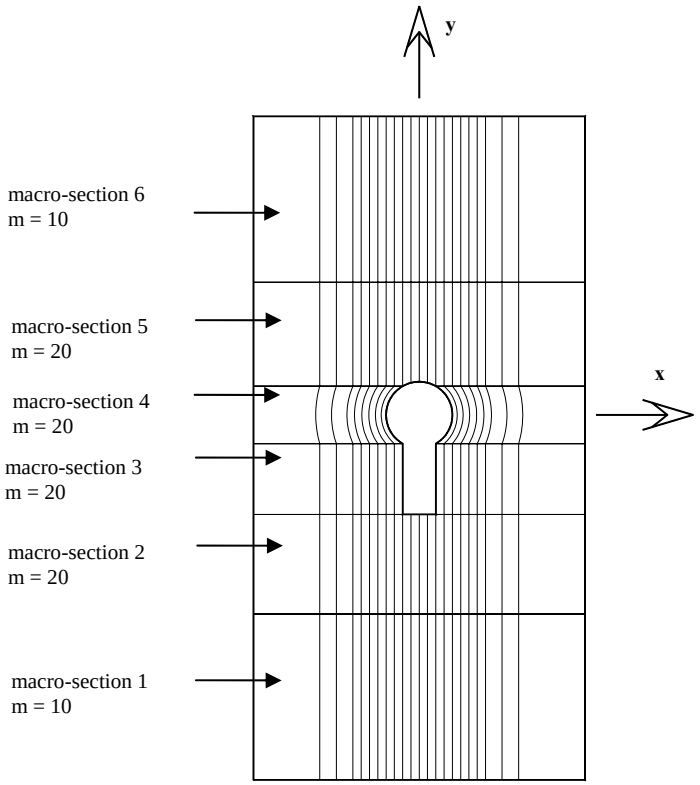

Fig. 22: Key-shaped hole: finite strip mesh.

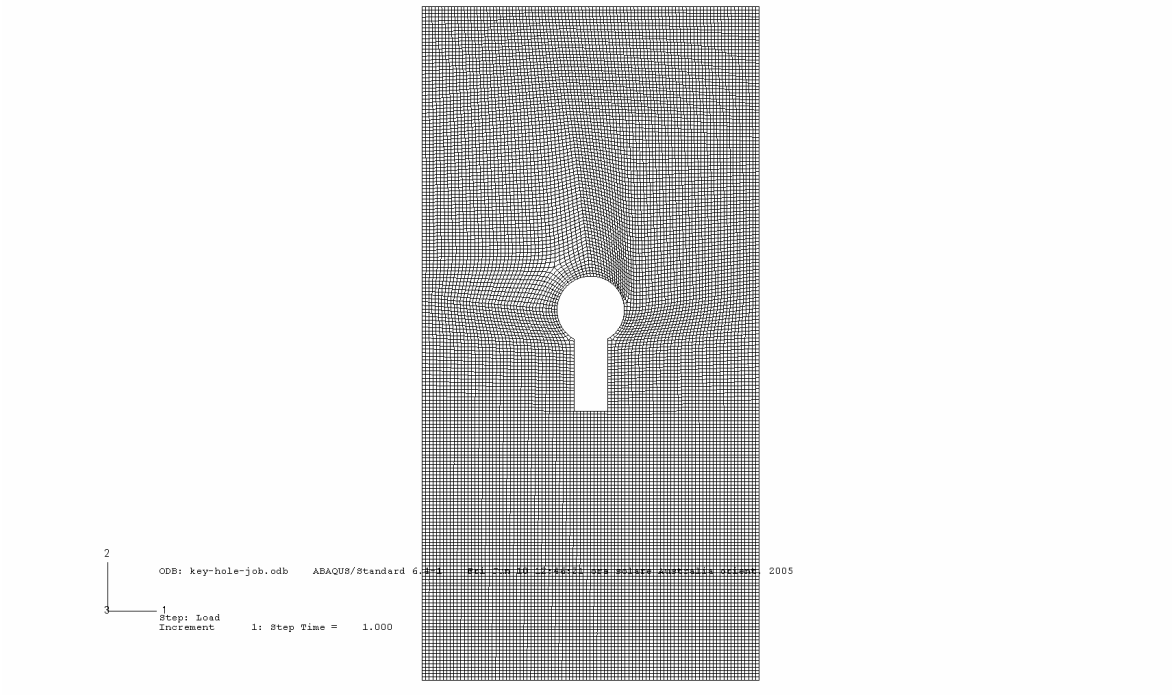

Fig. 23: Key-shaped hole: finite element mesh.

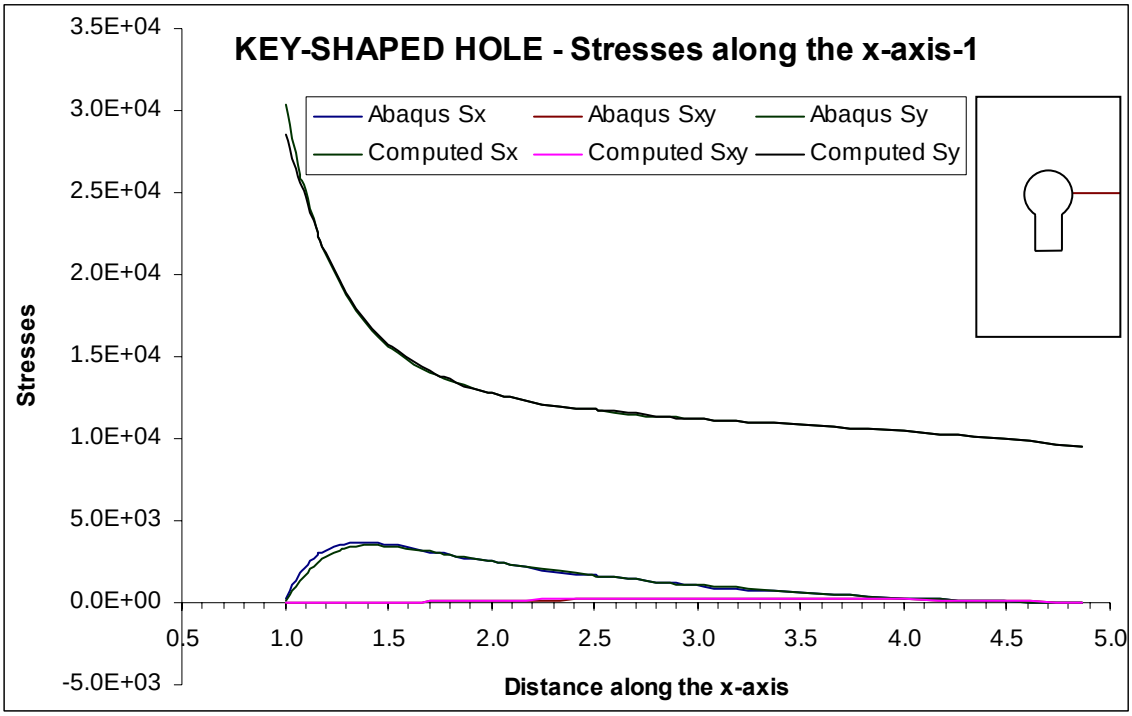

Fig. 24: Key-shaped hole: stress distribution along the symmetry x-axis-1.

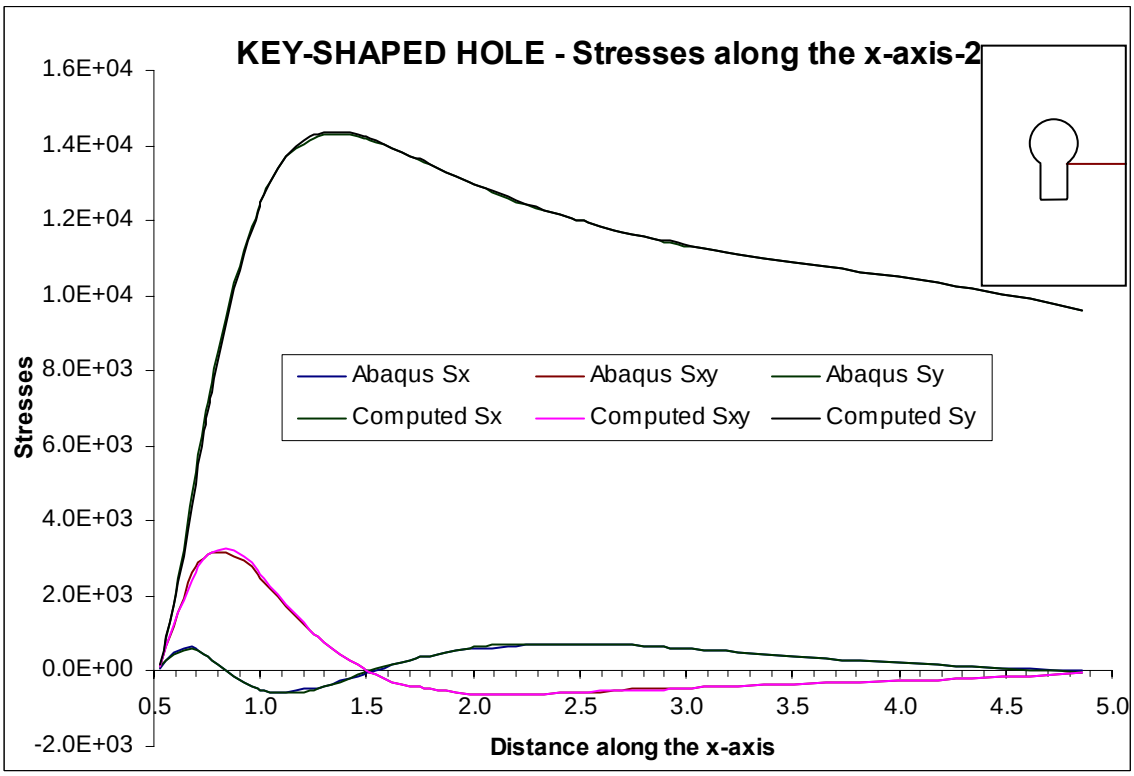

Fig. 25: Key-shaped hole: stress distribution along the x-axis-2.

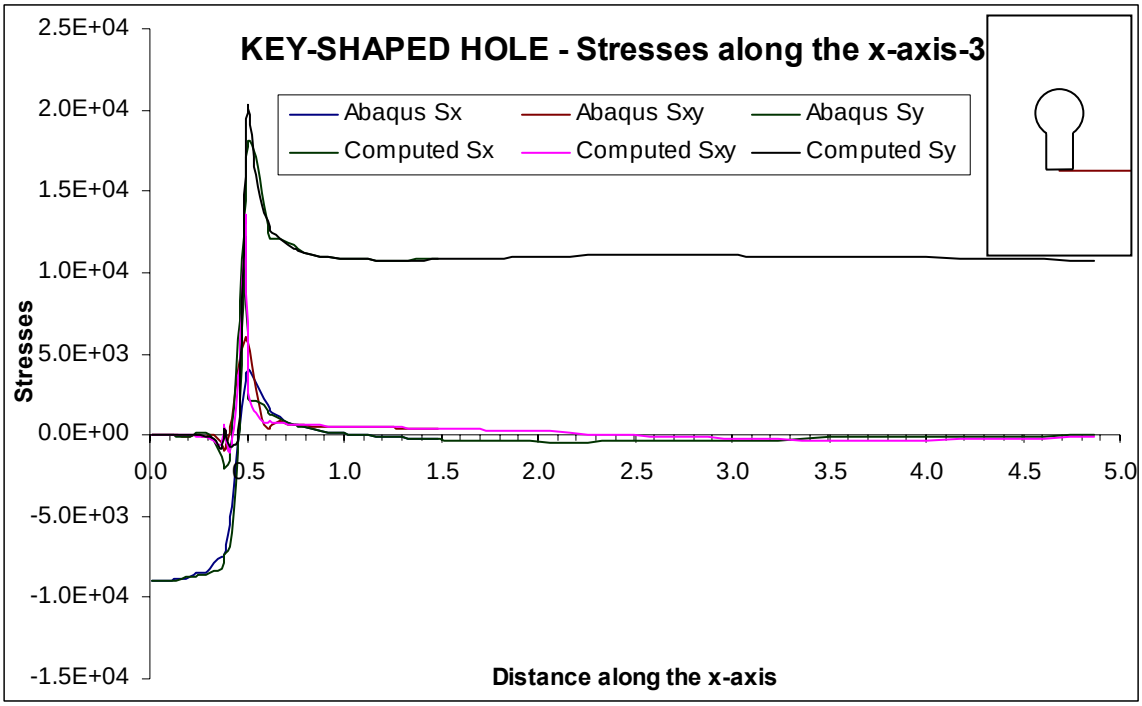

Fig. 26: Key-shaped hole: stress distribution along the x-axis-3.

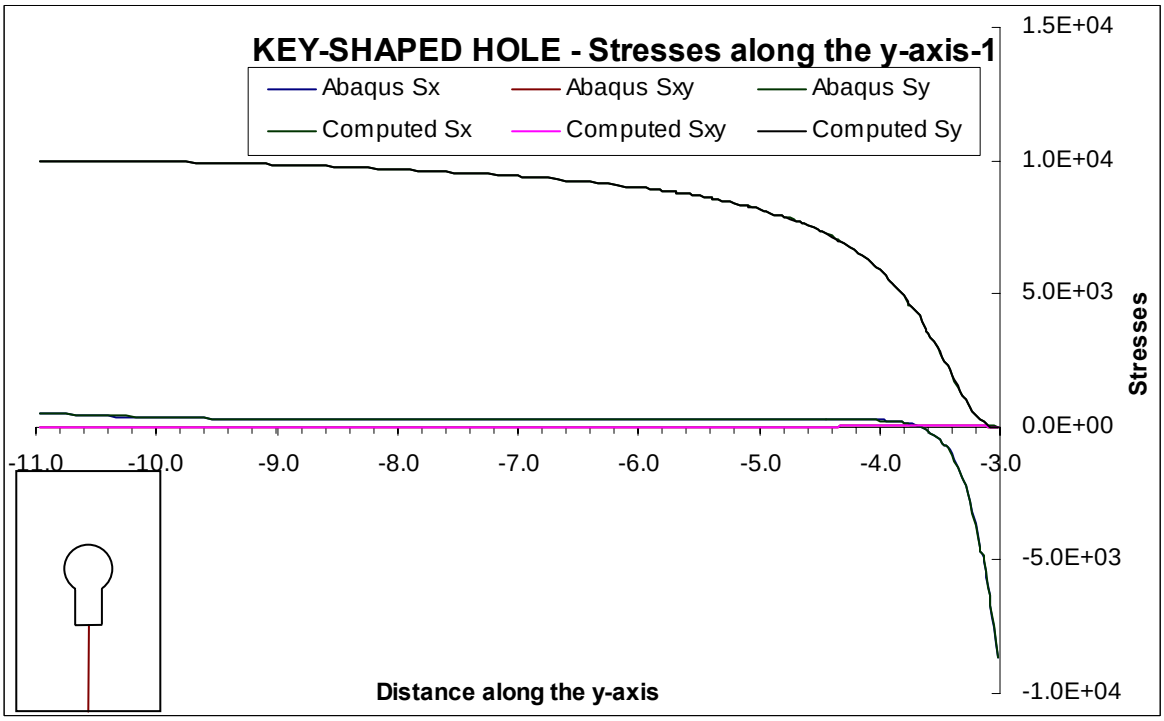

Fig. 27: Key-shaped hole: stress distribution along the symmetry y-axis-1.

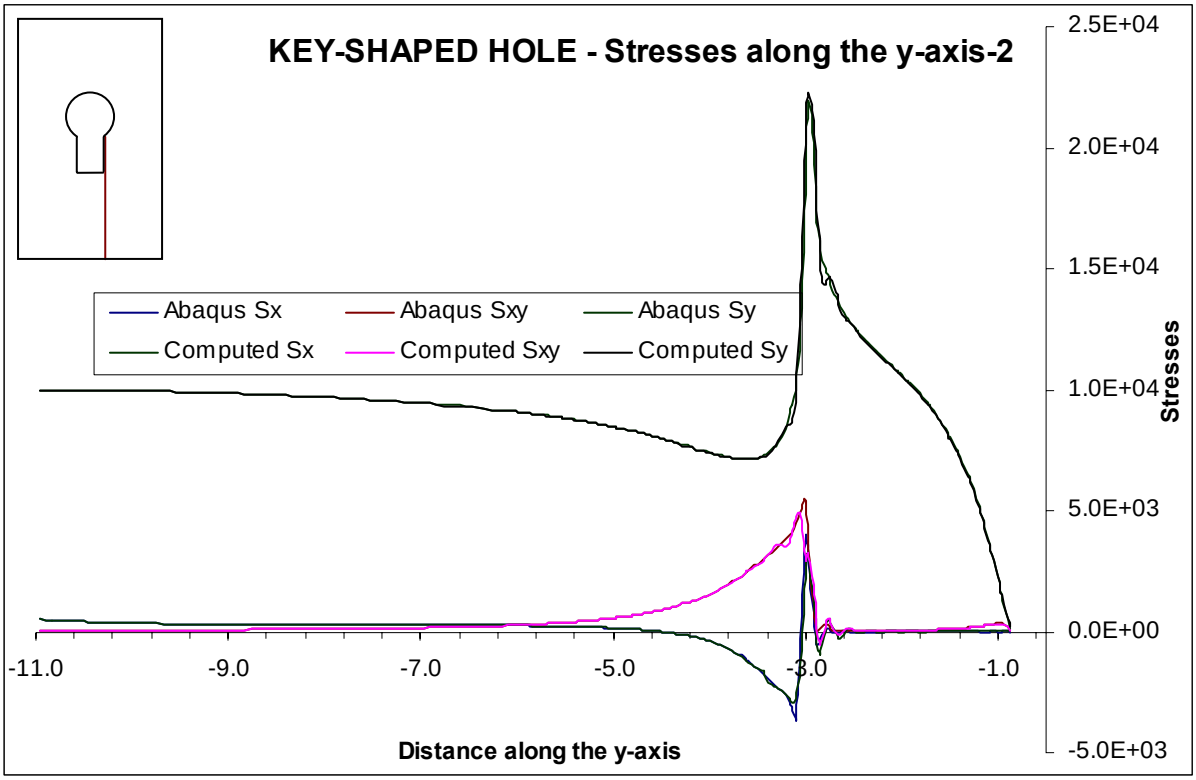

Fig. 28: Key-shaped hole: stress distribution along the y-axis-2.

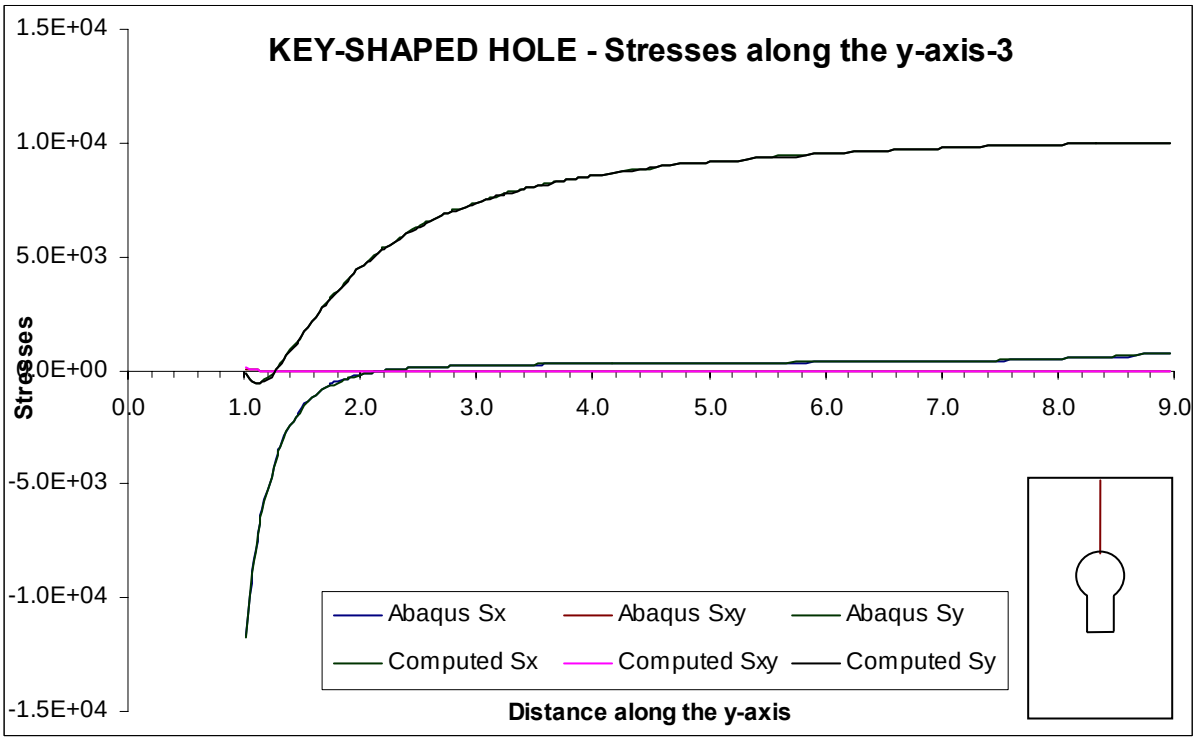

Fig. 29: Key-shaped hole: stress distribution along the y-axis-3.

5- Conclusions

A new development of the spline finite strip method has been presented. By introducing the so-called longitudinal assembly of strips, the present method has proved to be an efficient and reliable tool for the structural elastic analysis of plates of general geometry including perforations subjected to in-plane stress.
The derivation of the method, the mapping and the assembly process have been illustrated. Furthermore, three examples have demonstrated the accuracy of the isoparametric spline finite strip method in dealing with challenging problems like the stress amplification in a plate with circular hole, and the stress concentration in the proximity of the singular corner points of a rectangular cut-out. The reliability and efficiency of the method, which combines the flexibility of the finite element method with the small computational effort typical of the strip finite method, have been demonstrated by comparing results with theoretical solutions and finite element analysis results.

6- References

ABAQUS (2003). ABAQUS Reference Manual. Pawtucket, RI, USA.

Au, F. T. K. and Y. K. Cheung (1993). "Isoparametric spline finite strip for plane structures." Computers & Structures **48**(1): 23-32.

Baldassino, N., G. Eccher and R. Zandonini (2005). "Buckling design analysis of Thin-walled compressed members with or without perforations." International Journal of Steel Structures **5**(1): 33-42.

Cheung, Y. K. (1976). Finite strip method in structural analysis. Oxford; New York, Pergamon Press.

Cheung, Y. K. and F. T. K. Au (1995). "Isoparametric spline finite strip for degenerate shells." Thin-Walled Structures **21**(1): 65-92.

Cheung, Y. K., S. C. Fan and C. Q. Wu (1982). Spline finite strip in structural analysis. Proceedings of the International Conference on Finite Element Method, Shanghai, China.

Fan, S. C. (1982). Spline finite strip in structural analysis. Hong Kong, University of Hong Kong. **Ph.D.:** 314.

Godley, M. H. R. (1991). Storage Racking - chapter 11. Design of Cold Formed Steel Members, Ed. Rhodes**:** 361-399.

Lau, S. C. W. and G. J. Hancock (1986). "Buckling of thin flat-walled structures by a spline finite strip method." Thin-Walled Structures **4**(4): 269-294.

Leung, A. Y. T. and F. T. K. Au (1990). "Spline finite elements for beam and plate." Computers & Structures **37**(5): 717-729.

Rhodes, J. and M. Macdonald (1996). The effect of perforation length on the behaviour of perforated elements in compression. Thirthteenth International Speciality Conference on Cold-Formed Steel Structures.

Shanmugam, N. E. and M. Dhanalakshmi (2001). "State of art review and compilation of studies on perforated thin-walled structures." International Journal of Structural Stability and Dynamics **1**.

Shanmugam, N. E. and V. Thevendran (1991). "Lateral buckling of doubly symmetric beams containing openings." Journal of Engineering Mechanics, American Society of Civil Engineers **117**(7): 1427-1441.

Shanmugam, N. E., V. Thevendran and Y. H. Tan (1999). "Design formula for axially compressed perforated plates." Thin-Walled Structures **34**(1): 1.

Timoshenko, S. P. and J. N. Goodier (1970). Theory of Elasticity, McGraw-Hill.

Zienkiewicz, O. C. (1977). The finite element method. London; New York, McGraw-Hill.